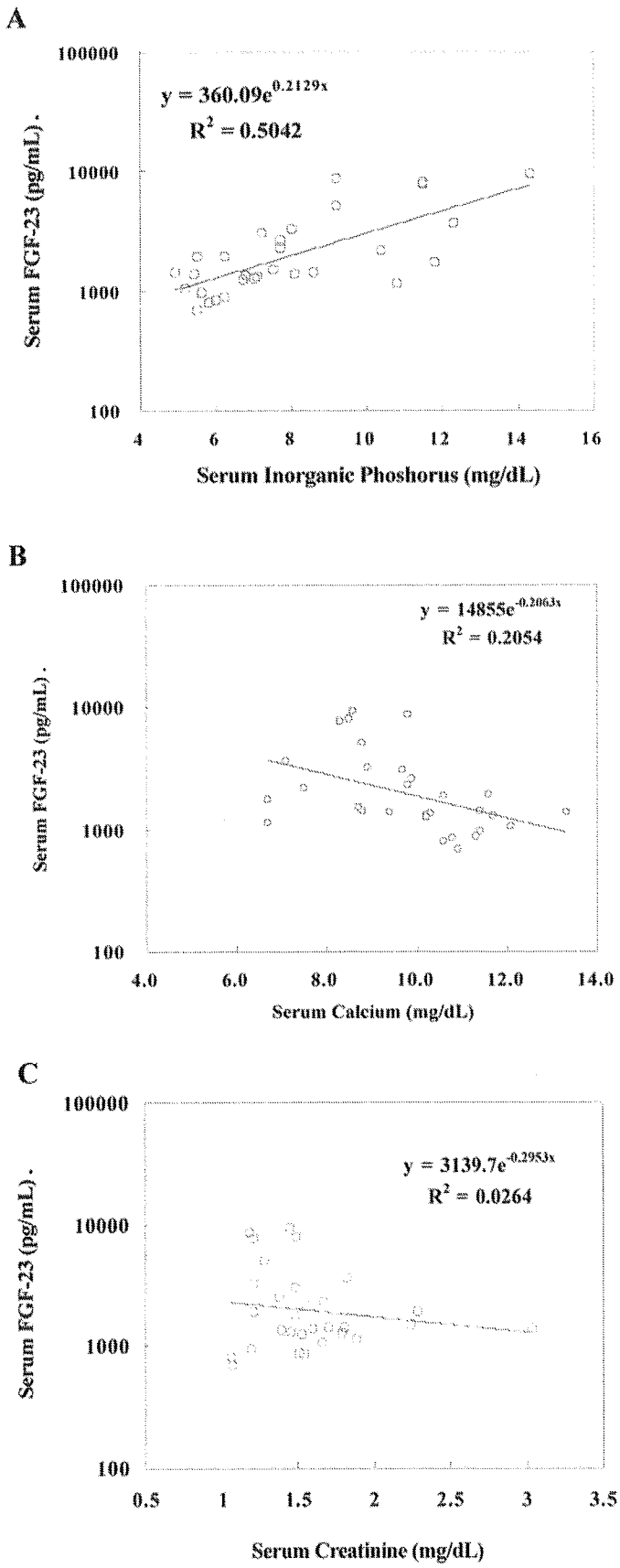

FIG. 4. **Correlations between serum FGF-23 and serum inorganic phosphorus (*A*), serum calcium (*B*), and serum creatinine (*C*) in 5/6 nephrectomized rats fed with P_i-controlled diet.** 5/6 nephrectomized rats were fed either high P_i, midrange P_i, or low P_i diet for 4 weeks. Serum creatinine, serum inorganic phosphorus, and serum FGF-23 were determined as described under "Experimental Procedures." Open circles represent the data from individual rats.

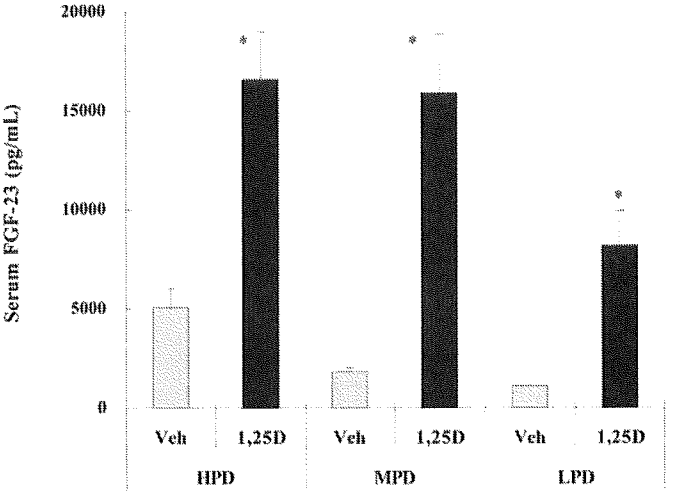

FIG. 5. **1α,25-Dihydroxyvitamin D_3 administration increased circulating FGF-23 in 5/6 nephrectomized rats.** 5/6 nephrectomized rats fed P_i-controlled diets were given either vehicle or 50 ng/kg 1α,25-dihydroxyvitamin D_3 intravenously, twice a week for 4 weeks. Serum FGF-23 was determined by ELISA. 1α,25-Dihydroxyvitamin D_3 injection to 5/6 nephrectomized rats induced a drastic increase in circulating FGF-23 among all diet groups. Each column represents mean ± S.E. (n = 10 rats/group). *, statistically significant difference between vehicle and 1α,25$(OH)_2D_3$ treated in each diet, $p < 0.05$ by Student's t test. *HPD*, high P_i diet; *MPD*, midrange P_i diet; *LPD*, low P_i diet.

as serum phosphorus. To evaluate the effect of 1α,25$(OH)_2D_3$ apart from serum phosphorus on FGF-23 production, 1α,25$(OH)_2D_3$ was administered to thyroparathyroidectomized rats with or without PTH infusion. 1α,25$(OH)_2D_3$ also increased serum FGF-23 in thyroparathyroidectomized, and the effect was independent of serum phosphorus (Fig. 2, *A–C*). The direct effect of 1α,25$(OH)_2D_3$ on FGF-23 production was confirmed by the fact that VDRKO mice did not respond to the 1α,25$(OH)_2D_3$ administration.

Larsson *et al.* (18) reported phosphate deprivation and/or phosphate loading to normal subjects did not affect serum FGF-23; however, serum phosphorus weakly correlated with serum FGF-23 in predialysis patients with chronic kidney disease. Recent studies also revealed that serum FGF-23 was elevated in patients with end-stage renal disease (16, 20, 28). In the present study, we investigated the effect of dietary phosphorus on FGF-23 production using 5/6 nephrectomized rats fed the diets with various kinds of phosphorus content. Serum FGF-23 was elevated in uremic rats; however, serum FGF-23 did not clearly correlate with serum creatinine in those rats as was observed in human subjects. Serum phosphorus was well controlled by the dietary phosphorus in 5/6 nephrectomized rats (Fig. 3*A*). Serum FGF-23 positively correlated with serum phosphorus in those rats (Fig. 3*C*). In the physiological condition, a high serum phosphorus suppresses 1α,25$(OH)_2D_3$ production in kidney. Thus, the elevation of serum FGF-23 induced by a high P_i diet was independent of serum 1α,25$(OH)_2D_3$. Moreover, serum FGF-23 was drastically elevated by 1α,25$(OH)_2D_3$ administration in 5/6 nephrectomized rats fed with various P_i-controlled diets (Fig. 5). However, serum FGF-23 did not correlate with serum calcium, serum creatinine, or serum PTH in those rats (Fig. 6, *B–D*). These observations suggested that FGF-23 production was mainly regulated by serum phosphorus and serum 1α,25$(OH)_2D_3$.

Recent studies (16, 17) reported that FGF-23 was elevated in some patients with XLH. Serum phosphorus concentrations were negatively correlated with circulating FGF-23 levels in patients with XLH. Moreover, FGF-23 mRNA expression was

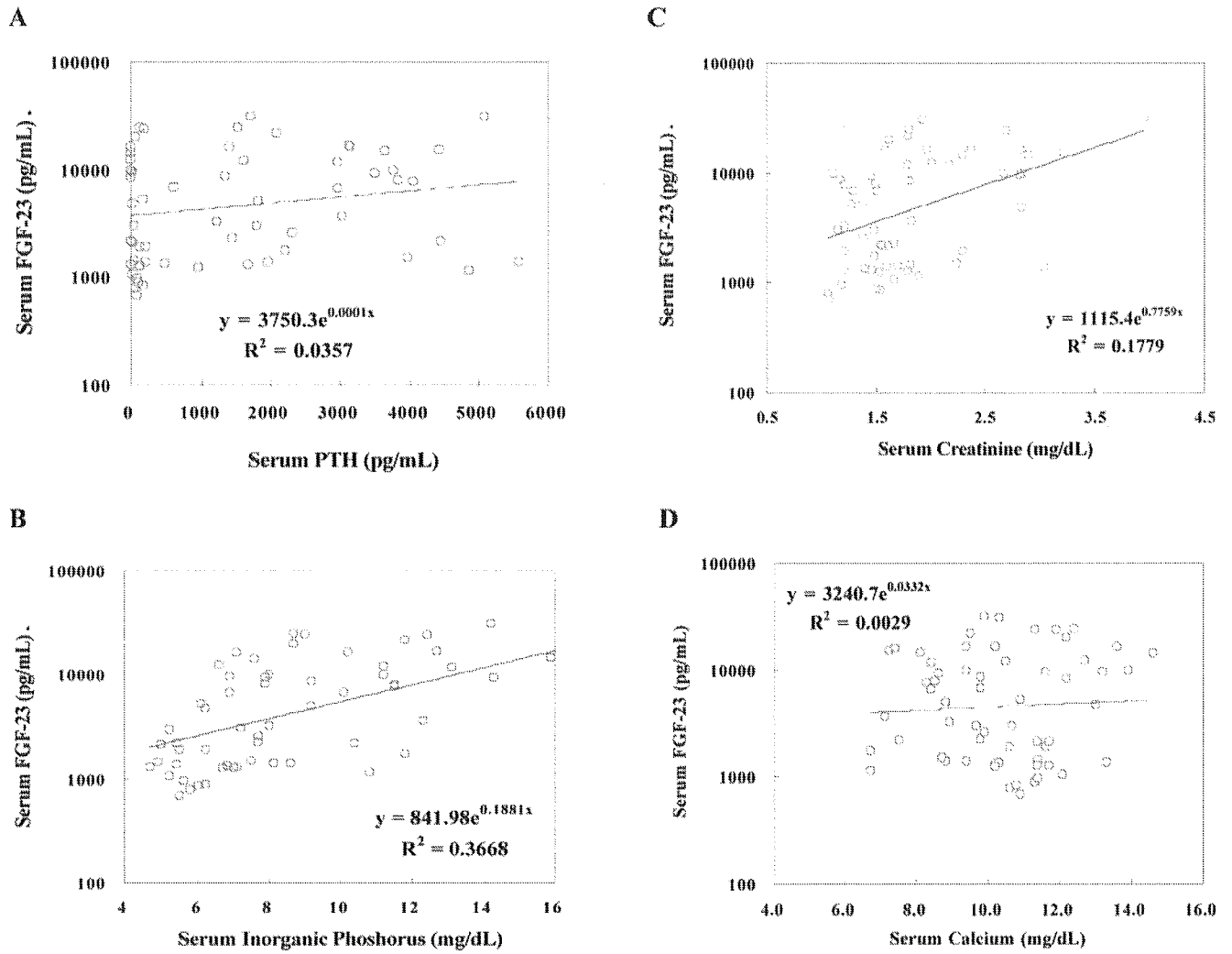

FIG. 6. **Correlations between serum FGF-23 and serum inorganic phosphorus (*A*), serum calcium (*B*), serum creatinine (*C*), and serum PTH (*D*) in 5/6 nephrectomized rats with or without 1α,25-dihydroxyvitamin D_3 administration.** 5/6 nephrectomized rats fed P_i-controlled diets were given intravenously either vehicle or 50 ng/kg 1α,25-dihydroxyvitamin D_3 for 4 weeks. Serum creatinine, serum inorganic phosphorus, and serum FGF-23 were determined as described under "Experimental Procedures." *Open circles* represent the data from individual rats.

enhanced in the calvarial and mandible bones of *Hyp*-mouse, which is a homologue of human XLH (13). Mutations in *PHEX*, a phosphate-regulating gene with homology to endopeptidase on the X-chromosome, are responsible for XLH. *PHEX* mRNA is predominantly expressed in bone and teeth. $1\alpha,25(OH)_2D_3$ decreased *PHEX* mRNA and *PHEX* protein in primary osteoblasts derived from newborn mouse calvaria as well as MC3T3-E1 cells, a mouse osteoblastic cell line, *in vitro* (29). In addition, *PHEX* mRNA expression in tibial bone was suppressed by $1\alpha,25(OH)_2D_3$ administration in 5/6 nephrectomized rats *in vivo* (30). It is plausible that administration of $1\alpha,25(OH)_2D_3$ up-regulated circulating FGF-23 levels in 5/6 nephrectomized rats at least partly by down-regulation of *PHEX* expression in bones.

FGF-23 induces hypophosphatemia by inhibiting both renal and intestinal P_i absorption by suppressing NaP_i-IIa and -IIb production (3, 12, 21, 22, 25). FGF-23 also inhibits $1\alpha,25(OH)_2D_3$ production in renal proximal tubules, which results in the reduction of intestinal P_i absorption and PTH secretion. On the contrary, $1\alpha,25(OH)_2D_3$ induced an increase in circulating FGF-23, and also loss of vitamin D signaling in VDRKO mice led to very low serum FGF-23. In 5/6 nephrectomized rats, serum phosphorus controlled by dietary phosphorus content positively correlated with serum FGF-23, suggesting an increase in serum phosphorus induces FGF-23 production. We propose that a feedback loop exists between serum phosphorus, $1\alpha,25(OH)_2D_3$, and FGF-23, in which the novel phosphate-regulating bone-kidney axis would be integrated with the parathyroid hormone-vitamin D_3 axis in regulating phosphate homeostasis.

Acknowledgments—We thank Keiko Kuroiwa and Yuko Azabu (Pharmaceutical Research Dept. II, Chugai Pharmaceutical Co., Ltd.) for their technical assistance. We also thank Dr. Paul Langman for his assistance with English usage.

REFERENCES

1. The ADHR Consortium (2000) *Nat. Genet.* **26,** 345–348
2. Yamashita, T., Yoshioka, M., and Ito, N. (2000) *Biochem. Biophys. Res. Commun.* **277,** 494–498
3. Shimada, T., Mizutani, S., Muto, T., Yoneya, T., Hino, R., Takeda, S., Takeuchi, Y., Fujita, T., Fukumoto, S., and Yamashita, T. (2001) *Proc. Natl. Acad. Sci. U. S. A.* **98,** 6500–6505
4. Berndt, T., Craig, T. A., Bowe, A. E., Vassiliadis, J., Reczek, D., Finnegan, R., Jan De Beur, S. M., Schiavi, S., and Kumar, R. (2003) *J. Clin. Invest.* **112,** 785–794
5. Rowe, P. S. N., de Zoysa, P. A., Dong, R., Wang, H. R., White, K. E., Econs, M. J., and Oudet, C. L. (2000) *Genomics* **67,** 54–68
6. Argiro, L. A., Desbarats, M., Glorieux, F. H., and Ecarot, B. (2001) *Genomics* **74,** 342–351
7. Jan De Beur, S. M., Finnegan, R., Vassiliadis, J., Cook, B., Barberion, D., Estes, S., Manavalan, P., Petroziello, J., Madden, S. L., Cho, J. Y., Kumar, R., Levine, M. A., and Schiavi, S. (2002) *J. Bone Miner. Metab.* **17,** 1102–1110
8. White, K. E., Jonsson, K. B., Carn, G., Hampton, G., Spector, T. D., Mannstadt, M., Lorenz-Depiereux, B., Miyauchi, A., Yang, M., Ljunggren, Ö., Meitinger, T., Strom, T. M., Jüppner, H., and Econs, M. J. (2001) *J. Clin.*

Endocrinol. Metab. **86,** 497–500
9. Gowen, L. C., Petersen, D. N., Mansolf, A. L., Qi, H., Stock, J. L., Tkalcevic, G. T., Simmons, H. A., Crawford, D. T., Chidsey-Frink, K. L., Ke, H. Z., McNeish, J. D., and Brown, T. A. (2003) *J. Biol. Chem.* **278,** 1998–2007
10. Quarles, L. D. (2003) *Am. J. Physiol.* **285,** E1–E9
11. Quarles, L. D. (2003) *J. Clin. Invest.* **112,** 642–646
12. Shimada, T., Muto, T., Urakawa, I., Yoneya, T., Yamazaki, Y., Okawa, K., Takeuchi, Y., Fujita, T., Fukumoto, S., and Yamashita, T. (2002) *Endocrinology* **143,** 3179–3182
13. Liu, S., Guo, R., Simpson, L. G., Xian, Z-S., Burnham, C. E., and Quarles, L. D. (2003) *J. Biol. Chem.* **278,** 37419–37426
14. Riminucci, M., Collins, M. T., Fedaeko, N. S., Cherman, N., Corsi, A., White, K. E., Waguespack, S., Gupta, A., Hannon, T., Econs, M. J., Bianco, P., and Robey, P. G. (2003) *J. Clin. Invest.* **112,** 683–692
15. Yamazaki, Y., Okazaki, R., Shibata, M., Hasegawa, Y., Satoh, K., Tajima, T., Takeuchi, Y., Fujita, T., Nakahara, K., Yamashita, T., and Fukumoto, S. (2002) *J. Clin. Endocrinol. Metab.* **87,** 4957–4960
16. Webber, T. J., Liu, S., Indridason, O. S., and Quarles, L. D. (2003) *J. Bone Miner. Res.* **18,** 1227–1234
17. Jonsson, K. B., Zahradnik, R., Larsson, T., White, K. E., Sugimoto, T., Imanishi, Y., Yamamoto, T., Hampson, G., Koshiyama, H., Ljuggren, Ö., Oba, K., Yang, I. M., Miyauchi, A., Econs, M. J., Lavigne, J., and Jüppner, H. (2003) *N. Eng. J. Med.* **348,** 1656–1663
18. Larsson, T., Nisbeth, U., Ljunggren, Ö., Jüppner, H., and Jonsson, K. B. (2003) *Kidney Int.* **64,** 2272–2279
19. Imanishi, Y., Inaba, M., Nakatsuka, K., Nagasue, K., Okuno, S., Yoshihara, A., Miura, M., Miyauchi, A., Kobayashi, K., Miki, T., Shoji, T., Ishimura, E., and Nishizawa, Y. (2004) *Kidney Int.* **65,** 1943–1946
20. Shigematsu, T., Kazama, J. J., Yamashita, T., Fukumoto, S., Hosoya, T., Geyjo, F., Fukagawa, M. (2004) *Am. J. Kidney Dis.* **44,** 250–256
21. Saito, H., Kusano, K., Kinosaki, M., Ito, H., Hirata, M., Segawa, H., Miyamoto, K., and Fukushima, N. (2003) *J. Biol. Chem.* **278,** 2206–2211
22. Bai, X. Y., Miao, D., Goltzman, D., and Karaplis, A. C. (2003) *J. Biol. Chem.* **278,** 9843–9849
23. Shimada, T., Urakawa, I., Yamazaki, Y., Hasegawa, H., Hino, R., Yoneya, T., Takeuchi, Y., Fujita, T., Fukumoto, S., and Yamashita, T. (2004) *Biochem. Biophys. Res. Comm.* **314,** 409–414
24. Shimada, T., Kakitani, M., Yamazaki, Y., Hasegawa, H., Takeuchi, Y., Fujita, T., Fukumoto, S., Tomizuka, K., and Yamashita, T. (2004) *J. Clin. Invest.* **113,** 561–568
25. Shimada, T., Hasegawa, H., Yamazaki, Y., Muto, T., Hino, R., Takeuchi, Y., Fujita, T., Nakahara, K., Fukumoto, S., and Yamashita, T. (2004) *J. Bone Miner. Res.* **19,** 429–435
26. Katai, K., Miyamoto, K., Kishida, S., Segawa, H., Nii, T., Tanaka, H., Tani, Y., Arai, H., Tatsumi, S., Morita, K., Taketani, Y., Takeda, E. (1999) *Biochem. J.* **343,** 705–714
27. Katai, K., Segawa, H., Haga, H., Morita, K., Arai, H., Tatsumi, S., Taketani, Y., Miyamoto, K., Hisano, S., Fukui, Y., and Takeda, E. (1997) *J. Biochem. (Tokyo)* **121,** 50–55
28. Yoshizawa, T., Handa, Y., Uematsu, Y., Takeda, S., Sekine, K., Yoshihara, Y., Kawakami, T., Arioka, K., Sato, H., Uchiyama, Y., Masushige, S., Fukamizu, A., Matsumoto, T., and Kato, S. (1997) *Nat. Genet.* **6,** 391–396
29. Ecarot, B., and Desbarats, M. (1999) *Endocrinology* **140,** 1192–1199
30. Brewer, A. J., Canaff, L., Hendy, G. F., and Tennenhouse, H. S. (2004) *Am. J. Physiol.* **286,** F739–F748

THE JOURNAL OF BIOLOGICAL CHEMISTRY
Vol. 280, No. 34, Issue of August 26, pp. 30511–30516, 2005
Printed in U.S.A.

Identification of the Amino Acid Residue of CYP27B1 Responsible for Binding of 25-Hydroxyvitamin D_3 Whose Mutation Causes Vitamin D-dependent Rickets Type 1*

Received for publication, May 12, 2005, and in revised form, June 22, 2005
Published, JBC Papers in Press, June 22, 2005, DOI 10.1074/jbc.M505244200

Keiko Yamamoto‡, Eriko Uchida§, Naoko Urushino§, Toshiyuki Sakaki¶‖, Norio Kagawa, Natsumi Sawada‡‡, Masaki Kamakura¶, Shigeaki Kato§§, Kuniyo Inouye§, and Sachiko Yamada‡¶¶**

*From the ‡Institute of Biomaterials and Bioengineering & School of Biomedical Sciences, Tokyo Medical and Dental University, 2-3-10 Kanda-Surugadai, Chiyoda-ku, Tokyo 101-0062, Japan, the §Division of Food Science and Biotechnology, Graduate School of Agriculture, Kyoto University, Sakyo-ku, Kyoto 606-8502, Japan, the ¶Biotechnology Research Center, Faculty of Engineering, Toyama Prefectural University, 5180 Kurokawa, Kosugi, Toyama 939-0398, Japan, the **Department of Biochemistry, Vanderbilt University School of Medicine, Nashville, Tennessee 37232-0146, the ‡‡Laboratory of Endocrinology and Molecular Metabolism, Graduate School of Nutritional Sciences, University of Shizuoka, 52-1 Yada, Shizuoka 422-8526, Japan, and the §§Institute of Molecular and Cellular Biosciences, Tokyo University, 1-1-1 Yayoi, Bunkyo, Tokyo 113-0032, Japan*

We previously reported the three-dimensional structure of human CYP27B1 (25-hydroxyvitamin D_3 1α-hydroxylase) constructed by homology modeling. Using the three-dimensional model we studied the docking of the substrate, 25-hydroxyvitamin D_3, into the substrate binding pocket of CYP27B1. In this study, we focused on the amino acid residues whose point mutations cause vitamin D-dependent rickets type 1, especially unconserved residues among mitochondrial CYPs such as Gln^{65} and Thr^{409}. Recently, we successfully overexpressed mouse CYP27B1 by using a GroEL/ES co-expression system. In a mutation study of mouse CYP27B1 that included spectroscopic analysis, we concluded that in a 1α-hydroxylation process, Ser^{408} of mouse CYP27B1 corresponding to Thr^{409} of human CYP27B1 forms a hydrogen bond with the 25-hydroxyl group of 25-hydroxyvitamin D_3. This is the first report that shows a critical amino acid residue recognizing the 25-hydroxyl group of the vitamin D_3.

The hormonally active form of vitamin D_3, 1,25-$(OH)_2D_3$,[1] plays essential roles in calcium homeostasis, immunology, and cell differentiation (1). 1,25-$(OH)_2D_3$ is produced by two-step hydroxylations at the 25-position in the liver by mitochondrial CYP27A1 and then at the 1α-position in the kidney by CYP27B1. The cDNA for CYP27B1 was first cloned in 1997 (2–5), and the sequence analysis of the CYP27B1 gene confirmed that defects in CYP27B1 cause vitamin D-dependent rickets type 1 (VDDR1). To date, 16 one-point mutants and several frameshift mutants have been reported (6–9). The mutated amino acid residues seemed to play important roles in the function of 1α-hydroxylase, such as substrate binding, activation of molecular oxygen, interaction with adrenodoxin, and folding of the P450 structure (10, 11).

To investigate the mutations in depth, spectral analyses including reduced CO-difference spectra and substrate-induced difference spectra are indispensable. However, the expression levels of wild type and CYP27B1 mutants were too low to carry out spectral analyses (11, 12). Thus, enhancement of the expression level of CYP27B1 is essential for structure-function analysis of CYP27B1. Recently, we successfully overexpressed mouse CYP27B1 by using a GroEL/ES co-expression system (13). The expression level of CYP27B1 is sufficient for the preparation of large amounts of wild type and CYP27B1 mutants for structural analyses. In addition, we successfully constructed a three-dimensional structure of CYP27B1 by the homology modeling technique using the structure of rabbit microsomal CYP2C5 as a template, which is the first solved x-ray structure as a eukaryotic CYP (14, 15). The three-dimensional model of CYP27B1 provided much information about the roles of amino acid residues at the mutated positions seen in VDDR1 patients. In this study, we focused on the mutants from VDDR1 whose mutated amino acids are not conserved among six mitochondorial P450s (Fig. 1). We demonstrate which amino acid residue is responsible for substrate binding by mutation studies that include spectral analysis of CYP27B1.

EXPERIMENTAL PROCEDURES

Materials—DNA modifying enzymes, restriction enzymes, and the DNA sequencing kit were purchased from Takara Shuzo Co., Ltd. (Kyoto, Japan). Primer DNAs for mutation were purchased from GENSET KK (Kyoto, Japan) (Table I). *Escherichia coli* DH5α (Takara Shuzo Co.) was used as a host strain. The pKSDdl was constructed from pkk223-3 as described previously (13). The GroEL/ES expression plasmid, pGro12, was kindly given by the HSP research laboratory (Kyoto, Japan). CHAPS was purchased from Dojindo (Kumamoto, Japan). NADPH was purchased from Oriental Yeast Co. (Tokyo, Japan). Bovine adrenodoxin and NADPH-adrenodoxin reductase were kindly given by Dr. Y. Nonaka of Koshien University. 25-$(OH)D_3$ was purchased from

* This work was supported in part by a grant-in-aid for Scientific Research from the Ministry of Education, Science and Culture of Japan and the Sankyo Foundation of Life Sciences. The costs of publication of this article were defrayed in part by the payment of page charges. This article must therefore be hereby marked "*advertisement*" in accordance with 18 U.S.C. Section 1734 solely to indicate this fact.

‖ To whom correspondence may be addressed: Biotechnology Research Center, Faculty of Engineering, Toyama Prefectural University, 5180 Kurokawa, Kosugi, Toyama 939-0398, Japan. Tel.: 81-766-56-7500; Fax: 81-766-56-7500; E-mail: tsakaki@pu-toyama.ac.jp.

¶¶ To whom correspondence may be addressed: Institute of Biomaterials and Bioengineering & School of Biomedical Sciences, Tokyo Medical and Dental University, 2-3-10 Kanda-Surugadai, Chiyoda-ku, Tokyo 101-0062, Japan. Tel.: 81-3-5280-8036; Fax: 81-3-5280-8005; E-mail: yamada.mr@tmd.ac.j.

[1] The abbreviations used are: 25-$(OH)D_3$, 25-hydroxyvitamin D_3; 1α,25-$(OH)_2D_3$, 1α,25-dihydroxyvitamin D_3; VDDR1, vitamin D-dependent rickets type 1; CYP, cytochrome P450; HPLC, high performance liquid chromatography; CHAPS, 3-[(3-cholamidopropyl)dimethylammonio]-1-propanesulfonic acid.

TABLE I
Oligonucleotides used as PCR primers to generate CYP27B1 mutants

Mutation	Oligonucleotides
S408I	5′-GATACGCTAGTCATCCTATGTCACTATGCC-3′
	5′-GGCATAGTGACATAGGATGACTAGCGTATC-3′
S408T	5′-GATACGCTAGTCACCCTATGTCACTATGCC-3′
	5′-GGCATAGTGACATAGGGTGACTAGCGTATC-3′
S408V	5′-GATACGCTAGTCGTCCTATGTCACTATGCC-3′
	5′-GGCATAGTGACATAGGACGACTAGCGTATC-3′
S408A	5′-GATACGCTAGTCGCCCTATGTCACTATGCC-3′
	5′-GGCATAGTGACATAGGGCGACTAGCGTATC-3′
Q65H	5′-GGCTGCATGAACTGCACGTGCATGGCGCTG-3′
	5′-CAGCGCCATGCACGTGCAGTTCATGCAGCC-3′
Q65E	5′-GGCTGCATGAACTGGAGGTGCATGGCGCTG-3′
	5′-CAGCGCCATGCACCTCCAGTTCATGCAGCC-3′
Q65A	5′-GGCTGCATGAACTGGCGGTGCATGGCGCTG-3′
	5′-CAGCGCCATGCACCGCCAGTTCATGCAGCC-3′
Q65L	5′-GGCTGCATGAACTGCTGGTGCATGGCGCTG-3′
	5′-CAGCGCCATGCACCAGCAGTTCATGCAGCC-3′
Q65N	5′-GGCTGCATGAACTGAATGTGCATGGCGCTG-3′
	5′-CAGCGCCATGCACATTCAGTTCATGCAGCC-3′

Wako Pure Chemical Industries, Ltd. (Osaka, Japan). Other chemicals used were of the highest quality commercially available.

Molecular Modeling and Substrate Docking—Molecular modeling and graphical manipulations were performed using SYBYL 6.9 (Tripos, St. Louis, MO). 25-Hydroxyvitamin D_3 was docked into the substrate binding pocket manually.

Construction of Expression Plasmids—The expression plasmid for mouse CYP27B1 with the His tag at the C terminus, pKCHis-m1α, was constructed as described (6). The expression plasmids for CYP27B1 mutants (S408I, S408T, S408V, S408A, Q65H, Q65E, Q65A, Q65L, Q65N) were generated by the QuikChange™ Site-directed Mutagenesis kit from Stratagene (Amsterdam, the Netherlands) according to the instruction manual. The oligonucleotide primers for mutagenesis are shown in Table I. Corrected generation of the desired mutations was confirmed by DNA sequencing.

Cultivation of the Recombinant E. coli Cells—The E. coli DH5α harboring pGro12 was transformed with the expression plasmid for wild type CYP27B1 (pKCHis-m1α) or its mutants. Recombinant *E. coli* cells were grown in TB media (pH 7.0) containing 50 μg/ml ampicillin and 25 μg/ml kanamycin at 26 °C under good aeration for 24 h. The induction of transcription of CYP27B1 cDNA and the GroEL/ES gene was initiated by addition of isopropyl 1-thio-β-D-galactopyranoside and arabinose at a final concentration of 1 mM and 4 mg/ml, respectively. δ-Aminolevulinic acid was also added at a final concentration of 1 mM.

Solubilization of Wild Type and CYP27B1 Mutants by CHAPS—The recombinant *E. coli* cells were suspended in 100 mM Tris-HCl buffer (pH 7.4) containing 1% CHAPS, 1 mM EDTA, 0.1 mM phenylmethylsulfonyl fluoride, and 20% glycerol, and disrupted by sonication for 15 min at 4 °C. Cell debris was removed at 1,200 × *g* for 10 min. Then the supernatant was ultracentrifugated at 100,000 × *g* for 1 h at 4 °C. The resultant supernatant was used for spectral and enzymatic analyses.

Measurement of Reduced CO-difference Spectra—Reduced CO-difference spectra were measured by a Shimadzu UV-2200 spectrophotometer (Kyoto, Japan) as described previously (16). The concentration of CYP27B1 was determined from the reduced CO-difference spectrum using a difference of extinction coefficient at 446 and 490 nm of 91 mM^{-1} cm^{-1} by Omura and Sato (17).

Measurement of Substrate-induced Difference Spectra—Substrate-induced difference spectra of wild type and CYP27B1 mutants were measured in the presence of 1.0 μM 25-(OH)D_3 by a Shimadzu UV-2200 spectrophotometer (Kyoto, Japan).

Western Blot Analysis of Gln^{65} Mutants—Anti-CYP27B1 antiserum was prepared using a purified sample of mouse CYP27B1 as antigen (13). The purified CYP27B1 (0.1 mg) was mixed with an equal volume of Freund's complete adjuvant and injected intradermally into a young male Japan White rabbit. At 2, 4, 6, and 8 weeks after the first injection, the rabbit was boosted with additional injections of 0.1 or 0.2 mg each of the antigen mixed with Freund's incomplete adjuvant.

The rabbit was bled 1 week after the final injection, and antiserum was prepared. The solubilized fractions of wild type and CYP27B1 mutants containing 0.6 μg of protein were subjected to electrophoresis on 5–20% linear gradient polyacrylamide sodium dodecyl sulfate gels, and transferred electrophoretically from the gel to poly(vinylidene difluoride) membrane. The membrane was probed with the anti-CYP27B1 antiserum mentioned above, and then reacted with horseradish peroxidase-labeled rabbit IgG. The immobilized proteins were detected by treating the membrane with a mixture of 4-chloro-1-naphtol and hydrogen peroxide.

	H	H	E	L	N	G,K,L	R	Y	P	S	C,H	I	P	C	G	R
VDDR	65	107	125	143	164	189	321	323	335	382	389	409	429	453	478	497
CYP27B1	Q	R	G	P	D	E	T	S	R	P	R	T	R	R	V	P
CYP27A1	Q	R	G	Q	D	L	T	S	K	P	R	V	Q	R	V	P
CYP24	L	R	G	K	D	E	T	A	R	P	R	M	R	R	I	P
CYP11A1	H	R	G	Q	D	D	T	S	R	P	R	Q	D	R	V	P
CyP11B1	V	R	G	P	D	S	T	V	R	P	R	R	N	R	V	P
CYP11B2	M	R	G	P	D	S	T	A	R	P	R	Q	N	R	V	P

FIG. 1. **Comparison of the amino acid sequences of human CYP27B1 with other mitochondrial cytochromes P450 at the mutated positions seen in patients with VDDR1.** The amino acid residues that are identical and homologous in all the CYPs are shaded *dark* and *light*, respectively. The amino acid residues at the non-conserved position are surrounded by *open boxes*.

Measurement of Hydroxylation Activity Toward 25-(OH)D_3, 1α-(OH)D_3, and Vitamin D_3—The 1α-hydroxylation activity toward 25-(OH)D_3 was measured in a reconstituted system consisting of the solubilized CYP27B1 or each of its mutants (0.5–6.0 nM), 2.0 μM adrenodoxin, 0.2 μM NADPH-adrenodoxin reductase, 0.025–1.0 μM substrate, 100 mM Tris-HCl (pH 7.4), 1 mM EDTA, 0.2% glycerol, and 0.1% CHAPS in a final volume of 0.5 ml. The 25-hydroxylation activity toward 1α-(OH)D_3 was measured in a similar manner except for the concentrations of 1α-(OH)D_3 (0.05–1.0 μM) and CYP27B1 (2.5 nM) or S408V (50 nM). The vitamin D_3 metabolism was measured in a reconstituted system consisting of 2.0 μM adrenodoxin, 0.2 μM NADPH-adrenodoxin reductase, 46 nM of the purified sample of the wild type (13), or 50 nM of the purified sample of S408V, 1.0 μM vitamin D_3, 100 mM Tris-HCl (pH 7.4), 1 mM EDTA, 0.2% glycerol, and 0.1% CHAPS. The concentration of CHAPS was determined on the basis of our previous study (13). After incubation at 37 °C for 3 min, the reaction was initiated by adding NADPH at a final concentration of 1 mM. The reaction was terminated by adding 2 ml of chloroform/methanol (3:1, v/v). After extraction, the organic phase was recovered and dried. The resulting residue was solubilized with acetonitrile and applied to HPLC under the following conditions: column, YMC-Pack ODS-AM (4.6 × 300 mm) (YMC Co., Tokyo, Japan); column temperature, 40 °C; mobile phase, linear gradient of 70–100% acetonitrile aqueous solution per 15 min; flow rate, 1.0 ml/min; UV detection, 265 nm. The kinetic parameters, K_m and k_{cat}, were calculated by the nonlinear regression analysis using the KaleidaGraph (Synergy software).

Other Methods—The concentrations of vitamin D_3 derivatives were estimated by their molar extinction coefficient of 1.80×10^4 M^{-1} cm^{-1} at 264 nm (18). Total protein concentrations were determined by the Bradford method using bovine serum albumin as a standard. Mouse CYP27B1, human CYP27B1, and rabbit CYP2C5 were aligned by using ClustalW interfaced with Clustal X (version 1.81) for Windows.

RESULTS

Docking of 25-(OH)D_3 into CYP27B1—The three-dimensional structure of CYP27B1, which was constructed and reported in our previous paper (14), gave abundant insights in regards to the function of each residue. We are greatly interested in how the CYP27B1 recognizes 25-(OH)D_3 and binds it as a substrate. We noted amino acid residues whose point mutant cause VDDR1 (Fig. 1). Fig. 1 shows comparison of the residues of CYP27B1 with other human mitochondrial CYPs at the mutated positions seen in patients with VDDR1. Residues conserved in these CYPs are thought to be responsible for common roles among mitochondrial CYPs, whereas residues not conserved are thought to be involved in specific roles of each enzyme such as substrate binding. Thus, we focused on mutants Q65H, P143L, E189L, S323Y, T409I, and R429P. The three-dimensional structure of CYP27B1 demonstrated that P143L, E189L, S323Y, and R429P are responsible for protein folding as previously reported (14) (Fig. 2*a*). On the other hand, Gln^{65} and Thr^{409} are lining the end of broad cavity above heme in the three-dimensional model of CYP27B1 (Fig. 2*a*).

In the docking study of 25-(OH)D_3 into the pocket, it is important to determine the substrate binding site and the conformation of 25-(OH)D_3. Considering the importance of

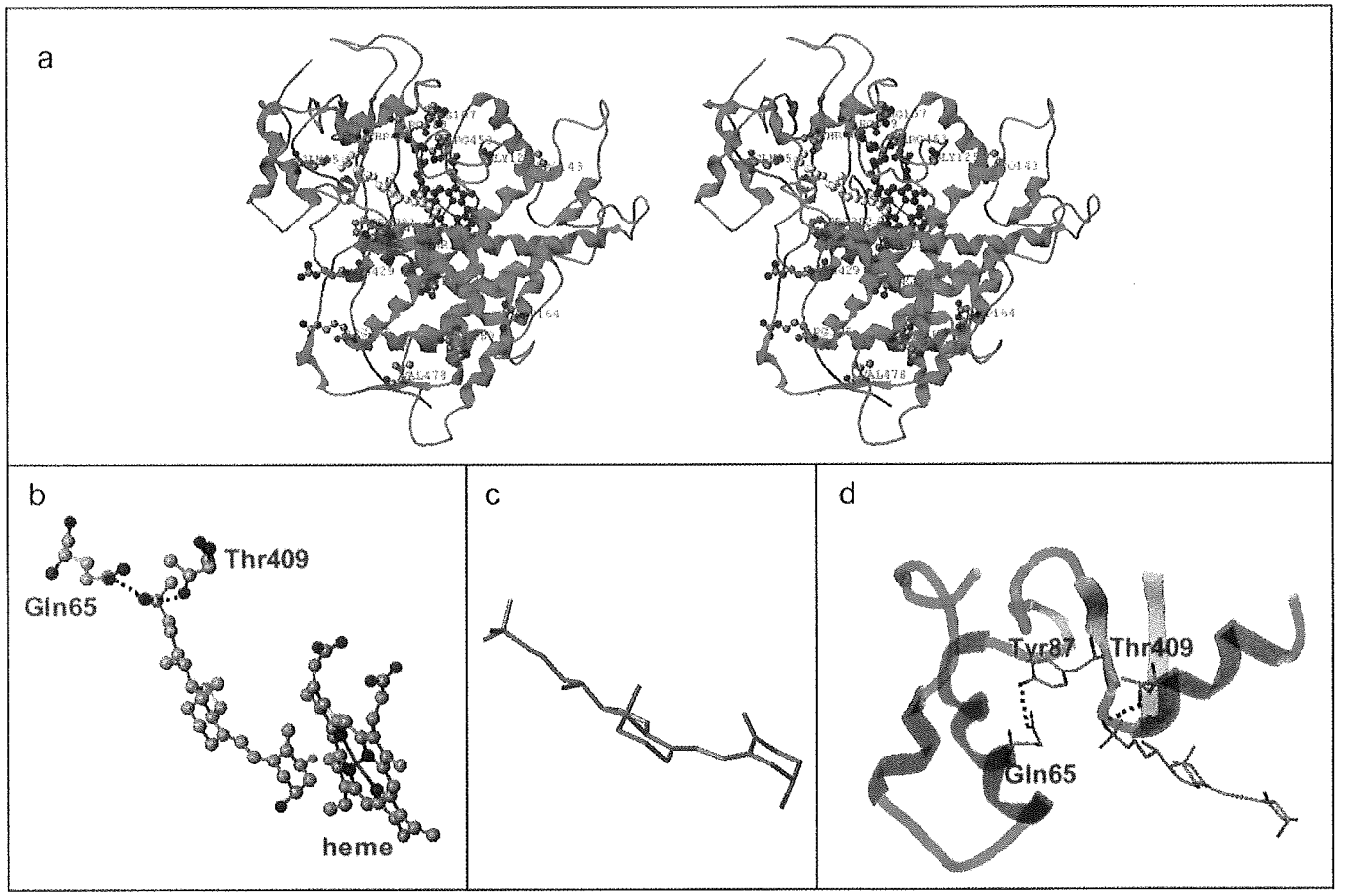

FIG. 2. *a*, stereo view of the complex model of human CYP27B1 and 25-(OH)D_3. Overall folding of CYP27B1 is represented by a *ribbon-loop* drawing. Sixteen amino acid residues where point mutation causes VDDR1 (atom type color), heme (*red*), and 25-(OH)D_3 (*yellow*) are depicted as a *ball and stick* model. *b*, the 25-hydroxyl group of 25-(OH)D_3 forms pincer-type hydrogen bond with Gln^{65} (2.83 Å) and Thr^{409} (2.82 Å), and the hydrogen at the 1α position (*cyan*), which will be subjected to hydroxylation, orients to an iron atom of the heme. The distance between C(1) and iron is 4.3 Å and that between hydrogen at the 1α-position and iron is 3.3 Å. *c*, conformation of 25-(OH)D_3 docked into the substrate binding pocket of CYP27B1. *d*, Gln^{65} may interact with Tyr^{87} on the β-sheet but not with the 25-hydroxyl group of the substrate.

Gln^{65} and Thr^{409} whose mutations cause VDDR1, we selected the substrate binding site where 25-(OH)D_3 can form the hydrogen bond between the 25-OH group and Gln^{65} and/or Thr^{409}. We docked 25-(OH)D_3 as follows: 1) the A-ring of 25-(OH)D_3 was superimposed on 1R-camphor accommodated in the substrate binding pocket of the P450cam protein (Protein Data Bank code 1DZ4) (19), because, structurally and biologically, the best characterized P450 is P450cam and we analyzed the docking modes of camphor into P450cam and found the modes being approximately conserved. In addition, P450cam belongs to the class 1 enzyme in the P450 superfamily as well as mitochondrial CYPs. 2) The side chain of 25-(OH)D_3 was positioned near Gln^{65} and Thr^{409}. 3) Spatial location of 25-(OH)D_3 was manually adjusted so as to minimize the van der Waals bump between the substrate vitamin and the amino acid residues lining the substrate binding pocket. The resulting structure of CYP27B1 and 25-(OH)D_3 complex is shown in Fig. 2*a*. The distances between the 25-hydroxyl group and Gln^{65} and the 25-hydroxyl group and Thr^{409} are 2.83 and 2.82 Å, respectively. This suggests that the 25-hydroxyl group forms pincer-type hydrogen bonds with Gln^{65} and Thr^{409}. The 1α-hydrogen of 25-(OH)D_3, which will be subjected to hydroxylation, orients to the iron atom as a constituent of heme in the CYP (Fig. 2*b*).

Conformation of 25-(OH)D_3 Accommodated in CYP27B1—As shown in Fig. 2*c*, 25-(OH)D_3 is docked with a stable conformation in which the A-ring adopts the chair form and the side chain adopts the gauche(+) conformation (43°) at C(16–17-20–22) and the following anti-conformation from C(20) to the terminal methyl group. A-ring adopts β-form. In this conformation, the distance between C(1) and iron is 4.3 Å and between hydrogen at the 1α-position and iron is 3.3 Å (Fig. 2*b*), which are consistent with the distances observed in the crystal structures: C(5)-iron (4.2 Å) and H(5)-iron (3.2 Å) in the camphor-P450cam complex (1DZ4) (19); C(5)-iron (3.9 Å) and H(5)-iron (3.3 Å) in the camphor-P450cam complex (1AKD) (20); C(1)-iron (3.8 Å) and H(1)-iron (2.9 Å) in the androstenedione-P450eryF complex (1EUP) (21). If the A-ring of 25-(OH)D_3 adopts the α-form, distances of C(1)-iron and C(2)-iron are 3.9 and 3.8 Å, respectively, resulting in the absence of a rational explanation for the selective hydroxylation that occurred at the 1α-position but not the 2-position. Thus, our docking model well explains the stereospecific hydroxylation at the 1α-position of 25-(OH)D_3.

Expression of Wild Type and CYP27B1 Mutants with GroEL/ES Co-expression System—Molecular modeling study of CYP27B1 strongly suggests that Ser^{408} of mouse CYP27B1 corresponding to Thr^{409} of human CYP27B1, and/or Gln^{65} are involved in substrate binding (Fig. 3). To reveal each function of the mutated amino acid residues, we generated multiple forms of CYP27B1 mutants at positions 408 (409 in human CYP27B1) and 65. As shown in Fig. 4, mutant S408I showed the reduced CO-difference spectra similar to wild type. S408T and S408A, and S408V, also showed similar spectra (data not shown). The expression level of the wild type of CYP27B1 was 200–300 nmol/liter of culture, as described previously (13). The

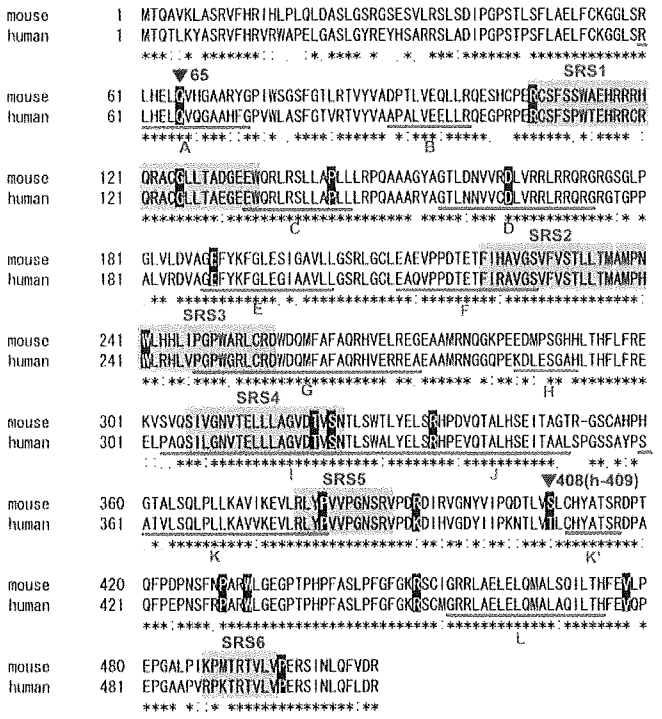

FIG. 3. **Sequence alignment of mouse and human CYP27B1.** The A to L helices are labeled as defined by Williams *et al.* (15). *Blue boxes* and *green bars* represent the substrate recognition site (*SRS*) and α-helix, respectively. *Black boxes* show the amino acid residues where the point mutation causes VDDR1.

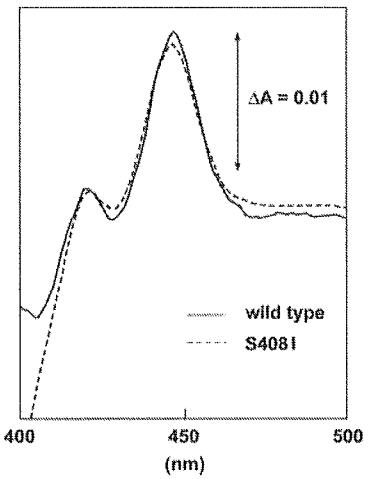

FIG. 4. **Reduced CO-difference spectra of wild type mouse CYP27B1 (—), and the mutant S408I (- - -).**

expression levels of Ser^{408} mutants, S408I and S408A, were nearly the same as the wild type, whereas those of S408T and S408V were higher (400–450 nmol/liter of culture). On the other hand, the expression levels of Gln^{65} mutants (Q65H, Q65E, Q65A, Q65L, Q65N) were too low to be determined by the reduced CO-difference spectra. However, Q65E showed a substrate-induced difference spectrum. Thus, the expression level of the Q65E hemoprotein was estimated to be 10 nmol/liter based on the assumption that Q65E shows a substrate-induced difference spectrum similar to wild type. In contrast, Western blot analysis showed that the distinct bands reacted with anti-CYP27B1 antiserum in the Gln^{65} mutants. The expression levels of the Gln^{65} mutants were not so different from that of the wild type (Fig. 5). These results suggest that most Gln^{65} mutants are expressed as apoproteins without a heme molecule in *E. coli* cells.

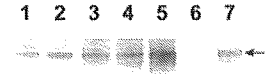

FIG. 5. **Western blot analysis of wild type and Gln^{65} mutants of mouse CYP27B1.** The solubilized fractions expressing each of the mutants Q65A (*lane 1*), Q65E (*lane 2*), Q65H (*lane 3*), Q65L (*lane 4*), Q65N (*lane 5*), control (*lane 6*: prepared from the control DH5α/pGro12 cells), and the wild type (*lane 7*) were analyzed as described under "Experimental Procedures."

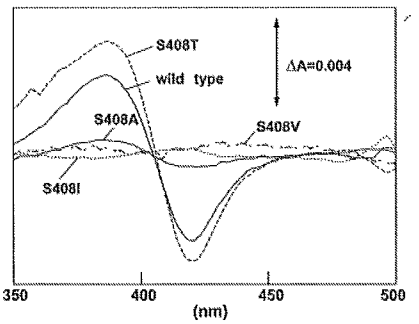

FIG. 6. **Substrate-induced difference spectra of wild type and CYP27B1 mutants with 1.0 μM 25-(OH)D_3.** The difference spectra of wild type and CYP27B1 mutants were measured in 100 mM Tris-HCl buffer (pH 7.4) containing 0.1% CHAPS. Enzyme concentrations were 160 nM (wild type, S408T, S408I) and 190 nM (S408A, S408V), respectively.

TABLE II
Kinetic parameters of wild type and CYP27B1 mutants for 25(OH)D_3 1α-hydroxylation activity

CYP27B1	k_{cat}	K_m	k_{cat}/K_m
	min^{-1}	μM	
Wild type	23.1 ± 0.9	0.28 ± 0.06	84 ± 19
S408T	5.9 ± 1.6	0.13 ± 0.03	46 ± 11
S408A	0.34 ± 0.06	0.24 ± 0.04	1.5 ± 0.3
S408V	0.78 ± 0.40	0.54 ± 0.18	1.5 ± 0.7
S408I	0.050 ± 0.020	0.18 ± 0.06	0.31 ± 0.10

TABLE III
Kinetic parameters of wild type and mutant S408V for 1α(OH)D_3 25-hydroxylation activity

CYP27B1	k_{cat}	K_m	k_{cat}/K_m
	min^{-1}	μM	
Wild type	0.60 ± 0.12	0.52 ± 0.05	1.1 ± 0.1
S408V	0.022 ± 0.010	0.66 ± 0.09	0.033 ± 0.009

Analysis of Substrate Binding of Wild Type and Ser^{408} Mutants of CYP27B1 with 25-(OH)D_3—As shown in Fig. 6, substrate-induced difference spectra of wild type and CYP27B1 mutants with 25-(OH)D_3 showed Type I spectra, indicating the change of spin state of heme iron of CYP27B1 from low spin to high spin. The magnitude of $\Delta A_{390-420}$ in S408T was slightly larger than the wild type of CYP27B1. In contrast, the magnitude of $\Delta A_{390-420}$ in S408V and S408A was quite small, but S408I showed no detectable spectral change. These results suggest that the substrate, 25-(OH)D_3, can remove the H_2O molecule as the sixth axial ligand of the heme iron of wild type CYP27B1 and mutant S408T. In addition, the hydroxyl group at the side chain of the amino acid at position 408 appears to be essential for removal of the H_2O molecule. It should be noted that S408I corresponding to T409I from patients with VDDR1 cannot remove the H_2O molecule by 25-(OH)D_3.

Analysis of 1α-Hydroxylation Activity of Wild Type and CYP27B1 Mutants toward 25-(OH)D_3—The 1α-hydroxylation activity toward 25-(OH)D_3 was examined using solubilized CYP27B1 by CHAPS as described under "Experimental Proce-

dures." As shown in Table II, kinetic parameters, K_m and k_{cat}, of the wild type CYP27B1 were estimated to be 0.28 μM and 23.1 min^{-1}, respectively. The k_{cat} and K_m values of S408T were significantly lower than those of the wild type CYP27B1. However, S408T appeared to have enough activity as a 1α-hydroxylase for 25-(OH)D_3 based on its k_{cat}/K_m value. On the other hand, S408A and S408V showed much smaller k_{cat} values than the wild type. As expected by spectral analysis, S408I showed the smallest activity among the mutants. Note that S408A, S408V, and S408I showed K_m values not so different from the wild type.

In the same way, 1α-hydroxylation activity toward 25-(OH)D_3 of Gln^{65} mutants was measured. Mutant Q65E showed only a small activity, although other Gln^{65} mutants showed no detectable activity. The K_m value of Q65E was estimated to be 0.80 μM, which is considerably higher than those of Ser^{408} mutants (Table II). Because the concentration of Q65E hemoprotein was not determined from reduced CO-difference spectrum probably because of its unstability, the k_{cat} value was not determined. On the assumption that Q65E shows a substrate-induced difference spectrum similar to wild type, k_{cat} was estimated to be 0.55 min^{-1}.

Analysis of 1α-(OH)D_3 25-Hydroxylation Activity of the Wild Type and S408V—We consider that the mutant T409I of human CYP27B1 corresponds to S408I of mouse CYP27B1. However, it might be possible that the conversion of Thr to Ile corresponds to the conversion of Ser to Val, judging from their chemical structure. Thus, enzymatic properties of S408V were compared with those of the wild type. As shown in Table III, the kinetic parameters, K_m and k_{cat}, of the wild type for 1α-(OH)D_3 25-hydroxylation was estimated to be 0.52 μM and 0.60 min^{-1}, respectively. Thus, the k_{cat}/K_m value was only 1.3% 1α-(OH)D_3 25-hydroxylation. Ser^{408} showed a similar K_m value but a much smaller k_{cat} value than wild type. These results are quite similar to those for 25-(OH)D_3 1α-hydroxylation, suggesting that Ser^{408} is involved in the binding of not only 25-(OH)D_3 but also 1α-(OH)D_3.

Vitamin D_3 Metabolism by the Wild Type and S408V—Fig. 7 shows the HPLC profiles of vitamin D_3 by wild type CYP27B1 and S408V. Both 1α-(OH)D_3 and 1-α,25(OH)$_2D_3$ were detected in the metabolism by the wild type. However, 25-(OH)D_3 was not detected as reported previously (13). On the other hand, S408V showed a clear peak of 25-(OH)D_3 in addition to those of 1α-(OH)D_3 and 1α,25-(OH)$_2D_3$. LC-MS analysis confirmed that this metabolite is 25-(OH)D_3 (data not shown). It is possible to assume that 25-(OH)D_3 is not detected as an intermediate because of its rapid conversion to 1α,25-(OH)$_2D_3$ by the wild type CYP27B1, but 25-(OH)D_3 is detected because of its slow conversion by S408V. Fig. 8 shows the time courses of vitamin D_3 metabolism. In the metabolism of wild type CYP27B1, 1α-(OH)D_3 increased up to 10 min and thereafter reached plateau, whereas 1α,25-(OH)$_2D_3$ continued increasing. On the other hand, 25-(OH)D_3 was not detected as described previously (13). In contrast, 25-(OH)D_3 was detected as a metabolite of vitamin D_3 by S408V. As shown in Fig. 7, 25-(OH)D_3 increased up to 10 min and thereafter reached plateau, whereas 1α-(OH)D_3 continued increasing. On the other hand, 1α,25-(OH)$_2D_3$ appeared at 10 min, and then the rate of 1α,25-(OH)$_2D_3$ formation increased with increasing time. Vitamin D_3 metabolism together with 25-(OH)D_3 1α-hydroxylation and 1α-(OH)D_3 25-hydroxylation by S408V strongly indicated that S408V has a dual pathway to produce 1α,25-(OH)$_2D_3$ from vitamin D_3 as shown in Fig. 9. Although 25-(OH)D_3 was not detected in the wild type-dependent metabolism of vitamin D_3, it is possible that the wild type has a dual pathway as well as S408V.

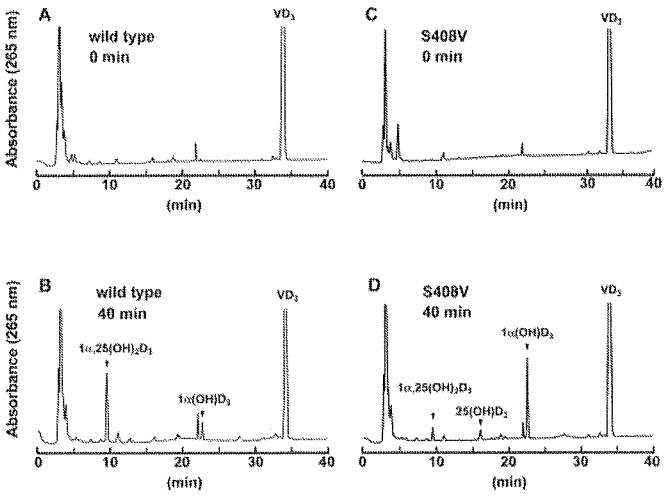

FIG. 7. **HPLC profiles of vitamin D_3 and its metabolites by the wild type (*A* and *B*) and S408V (*C* and *D*).** The metabolites at 0 min (*A* and *C*) and 40 min (*B* and *D*) were analyzed by HPLC according to "Experimental Procedures."

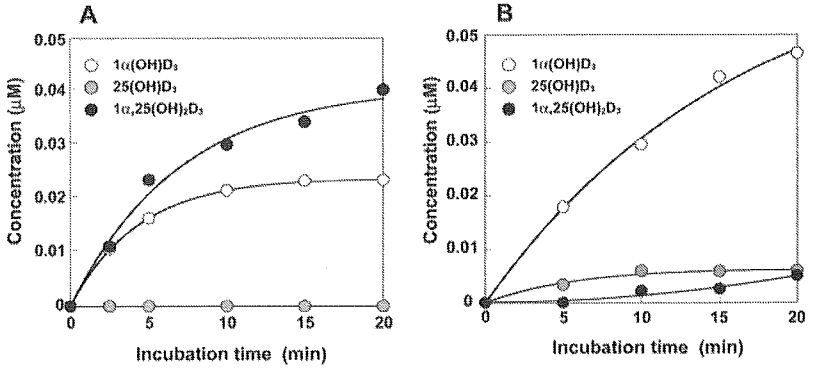

FIG. 8. **Time courses of vitamin D_3 metabolism by wild type (*A*) and S408V (*B*).** The amounts of metabolites of vitamin D_3 at 5, 10, 15, and 20 min was measured according to "Experimental Procedures."

DISCUSSION

Kitanaka *et al.* (6, 7) cloned eight types of missense mutations and one nonsense mutation from Japanese VDDR1 patients, and other groups identified nine missense mutations from patients (8, 9). None of the CYP27B1 mutants expressed in mammalian cells (6) and *E. coli* cells (11, 12) showed 1α-hydroxylase activity toward 25-(OH)D_3. Thus, the mutated amino acid residues seemed to play important roles in the function of 1α-hydroxylase. Our previous study (11) suggested that Arg^{107}, Gly^{125}, and Pro^{497} destroyed the tertiary structure of the substrate-heme pocket. It was also suggested that Arg^{389} and Arg^{453} of CYP27B1 were involved in heme-propionate binding and that Asp^{164} stabilized the 4-helix bundle consisting of D, E, I, and J helices, possibly by forming a salt bridge. Thr^{321} was found to be responsible for the activation of molecular oxygen.

As shown in Fig. 1, amino acid residues at positions 65, 143,

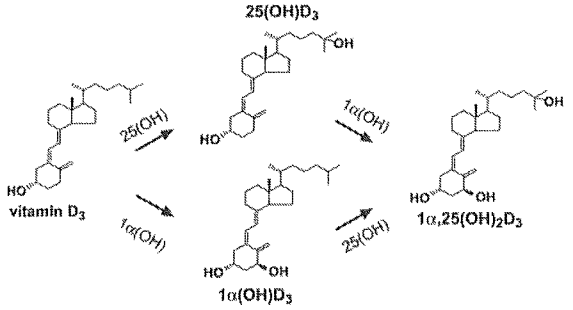

FIG. 9. **Metabolic pathway of vitamin D_3 by CYP27B1 and the mutant S408V.**

189, 323, 409, and 429 of human CYP27B1 were not conserved among mitochondorial P450s. Of these mutations, P143L, E189G(K,L), and R429P are assumed to disrupt protein folding because Pro and Gly residues are known to be helix breakers. In addition, S323Y in the I helix appears to play an important role in protein folding because the side chain of the amino acid residue at position 323 is oriented to the opposite side of a heme molecule, buried inside the protein structure (14). The three-dimensional structure model of CYP27B1 implied that Gln^{65} and/or Thr^{409} interacts with 25-(OH)D_3, probably by forming a hydrogen bond with the 25-hydroxyl group of the substrate. We have not successfully overexpressed human CYP27B1 yet, but we have successfully overexpressed mouse CYP27B1 by using a GroEL/ES co-expression system. Thus, we generated mouse CYP27B1 mutants for Gln^{65} and Ser^{408}, corresponding to Thr^{409} of human CYP27B1. The substitution of Ser^{408} to Thr did not cause significant alterations in substrate binding and 1α-hydroxylation activity toward 25-(OH)D_3. However, the substitutions to Ala, Val, and Ile dramatically decreased 1α-hydroxylation activity and changed the substrate binding manner. Judging from the K_m values of S408A, S408V, and S408I, these mutants have significant affinity for 25-(OH)D_3. However, based on their substrate-induced manner, their binding mode of the substrate appears unsuitable for displacement of H_2O as the distal ligand. Because the displacement of the H_2O molecule by the substrate is essential for P450 reactions, good correlation between the magnitude of $\Delta A_{390-420}$ in Fig. 5 and k_{cat} value in Table II is quite reasonable. Note that S408V has much lower activity than S408T. The difference in the side chain of Val from Thr is the difference between a methyl and a hydroxyl group. Thus, the hydroxyl group is responsible for substrate binding for the P450 reaction. It is possible to assume that the hydroxyl group of Ser^{408} of mouse CYP27B1 or Thr^{409} of human CYP27B1 interacts with the 25-OH group of the substrate through a hydrogen bond. The high affinity of S408A, S408V, and S408I for 25-(OH)D_3 may suggest that another amino acid residue takes the place of Ser^{408} through a hydrogen bond with the substrate.

It is noted that not only 25-(OH)D_3 1α-hydroxylation but also 1α-(OH)D_3 25-hydroxylation by S408V was much less than those of the wild type CYP27B1. These results suggest that the hydroxyl group of Ser^{408} of mouse CYP27B1 is involved in substrate binding of both substrates. Note that the substrate is fixed in the opposite direction in the substrate binding pocket of CYP27B1 between 1α- and 25-hydroxylations. Thus, it appears that the hydroxyl group of Ser^{408} interacts with the 1α-hydroxyl group of 1α-(OH)D_3. On the other hand, 1α-hydroxylation and 25-hydroxylation activities of S408V toward vitamin D_3 appear to be similar to those of the wild type, based on the time courses of the metabolites shown in Fig. 7. These results are consistent with the fact that vitamin D_3 has no hydroxyl groups at positions C-1α and C-25 to interact with the hydroxyl group of the amino acid at position 408.

The significantly higher K_m and lower k_{cat} values of Q65E than the wild type are consistent with an involvement of Gln^{65} in binding of the substrate. However, Western blot and spectral analyses of Gln^{65} mutants indicated that most Gln mutants were expressed as apoproteins without heme molecules, whereas Q65E showed a small amount of hemoprotein and the activity. These results strongly suggest that Gln^{65} is involved in protein folding.

In this study, we revealed that Ser^{408} and Gln^{65} play important roles in substrate binding and the folding of mouse CYP27B1, respectively. The reasons why mutations T409I and Q65H of human CYP27B1 cause VDDR1 were also clearly understood. It is noteworthy that the predictions derived from the three-dimensional model showed good agreement with the experimental data. Thus, this three-dimensional model gives essential information on the structure-function relationship of CYP27B1.

REFERENCES

1. Feldman, D., Glorieux, F. H., and Pike, J. W. (eds) (1997) *Vitamin D*, Academic Press, New York
2. Takeyama, K., Kitanaka, S., Sato, T., Kobori, M., Yanagisawa, J., and Kato, S. (1997) *Science* **277,** 1827–1830
3. Fu, G. K., Lin, D., Zhang, M. Y. H., Bikle, D. D., Shackleton, C. H. L., Miller, W. L., and Portale, A. A. (1997) *Mol. Endocrinol.* **11,** 1961–1970
4. Shinki, T., Shimada, H., Wakino, S., Anazawa, H., Hayashi, M., Saruta, T., DeLuca, H. F., and Suda, T. (1997) *Proc. Natl. Acad. Sci. U. S. A.* **94,** 12920–12925
5. St-Arnaud, R., Messerlian, S., Moir, J. M., Omdahl, J. L., and Glorieux, F. H. (1997) *J. Bone Miner. Res.* **12,** 1552–1559
6. Kitanaka, S., Takeyama, K., Murayama, A., Sato, T., Okumura, K., Nogami, M., Hasegawa, Y., Niimi, H., Yanagisawa, J., Tanaka, T., and Kato, S. (1998) *N. Engl. J. Med.* **338,** 653–661
7. Kitanaka, S., Murayama, A., Sakaki, T., Inouye, K., Seino, Y., Fukumoto, S., Shima, M., Yukizane, S., Takayanagi, M., Niimi, H., Takeyama, K., and Kato, S. (1999) *J. Clin. Endocrine Metab.* **84,** 4111–4117
8. Portale, A. A., and Miller, W. L. (2000) *Pediatr. Nephrol.* **14,** 620–625
9. Yoshida, T., Monkawa, T., Tenenhouse, H. S., Goodyer, P., Shinki, T., Suda, T., and Wakino, S. (1998) *Kidney Int.* **54,** 1437–1443
10. Omdahl, J. L., Borovnikova, Choe, S., Dwivedi, P. P., and May, B. K. (2001) *Steroids* **66,** 381–389
11. Sawada, N., Sakaki, T., Kitanaka, S., Kato, S., and Inouye, K. (2001) *Eur. J. Biochem.* **268,** 6607–6615
12. Sawada, N., Sakaki, T., Kitanaka, S., Takeyama, K., Kato, S., and Inouye, K. (1999) *Eur. J. Biochem.* **265,** 950–956
13. Uchida, E., Kagawa, N., Sakaki, T., Urushino, N., Sawada, N., Kamakura, M., Ohta, M., Kato, S., and Inouye, K. (2004) *Biochem. Biophys. Res. Commun.* **323,** 505–511
14. Yamamoto, K., Masuno, H., Sawada, N., Sakaki, T., Inouye, K., Ishiguro, M., and Yamada, S. (2004) *J. Steroid Biochem. Mol. Biol. 89-90,* 167–171
15. Williams, P. A., Comse, J., Sridhar, V., Johnson, E. F., and McRee, D. E. (2000) *Mol. Cell* **5** 121–131
16. Kondo, S., Sakaki, T., Ohkawa, H., and Inouye, K. (1999) *Biochem. Biophys. Res. Commun.* **257,** 273–278
17. Omura, T., and Sato, R. (1964) *J. Biol. Chem.* **118,** 397–404
18. Hiwatashi, A., Nishi, Y., and Ichikawa, Y. (1982) *Biochem. Biophys. Res. Commun.* **105,** 320–327
19. Schlichting, I., Berendzen, J., Chu, K., Stock, A. M., Maves, S. A., Benson, D. E., Sweet, R. M., Ringe, D., Petsko, G. A., and Sligar, S. G. (2000) *Science* **287,** 1615–1622
20. Schlichting, I., Jung, C., and Schulze, H. (1997) *FEBS Lett.* **415,** 253–257
21. Cupp-Vickery, J., Anderson, R., and Hatziris, Z. (2000) *Proc. Natl. Acad. Sci. U. S. A.* **97,** 3050–3055

Role of the vitamin D receptor in FGF23 action on phosphate metabolism

Yoshio INOUE*†, Hiroko SEGAWA*, Ichiro KANEKO*, Setsuko YAMANAKA*, Kenichiro KUSANO‡, Eri KAWAKAMI*, Junya FURUTANI*, Mikiko ITO*, Masashi KUWAHATA*, Hitoshi SAITO‡, Naoshi FUKUSHIMA‡, Shigeaki KATO§, Hiro-omi KANAYAMA† and Ken-ichi MIYAMOTO*[1]

*Department of Molecular Nutrition, Institute of Health Bioscience, The University of Tokushima Graduate School, Kuramoto-cho 3, Tokushima 770-8503, Japan, †Department of Urology, The University of Tokushima School of Medicine, 3-18-15, Kuramoto-Cho, Tokushima 770-8503, Japan, ‡Chugai Pharmaceutical Co. Ltd., Gotenba 412-8513, Japan, and §Institute of Molecular and Cellular Biosciences, University of Tokyo, Yayoi 1-1-1, Bunkyo-ku, Tokyo 113-0032, Japan

FGF23 (fibroblast growth factor 23) is a novel phosphaturic factor that influences vitamin D metabolism and renal re-absorption of P_i. The goal of the present study was to characterize the role of the VDR (vitamin D receptor) in FGF23 action using VDR(−/−) (VDR null) mice. Injection of FGF23M (naked DNA encoding the R179Q mutant of human FGF23) into VDR(−/−) and wild-type VDR(+/+) mice resulted in an elevation in serum FGF23 levels, but had no effect on serum calcium or parathyroid hormone levels. In contrast, injection of FGF23M resulted in significant decreases in serum P_i levels, renal Na/P_i co-transport activity and type II transporter protein levels in both groups when compared with controls injected with mock vector or with FGFWT (naked DNA encoding wild-type human FGF23). Injection of FGF23M resulted in a decrease in 25-hydroxyvitamin D 1α-hydroxylase mRNA levels in VDR(−/−) and VDR(+/+) mice, while 25-hydroxyvitamin D 24-hydroxylase mRNA levels were significantly increased in FGF23M-treated animals compared with mock vector control- or FGF23WT-treated animals. The degree of 24-hydroxylase induction by FGF23M was dependent on the VDR, since FGF23M significantly reduced the levels of serum $1,25(OH)_2D_3$ [1,25-hydroxyvitamin D_3] in VDR(+/+) mice, but not in VDR(−/−) mice. We conclude that FGF23 reduces renal P_i transport and 25-hydroxyvitamin D 1α-hydroxylase levels by a mechanism that is independent of the VDR. In contrast, the induction of 25-hydroxyvitamin D 24-hydroxylase and the reduction of serum $1,25(OH)_2D_3$ levels induced by FGF23 are dependent on the VDR.

Key words: fibroblast growth factor 23, kidney, phosphate transport, vitamin D receptor.

INTRODUCTION

P_i (inorganic phosphate) is required for cellular function and skeletal mineralization. P_i re-absorption in the renal proximal tubule is a major mechanism in the maintenance of overall P_i homoeostasis; it is a Na^+-dependent, secondary active process involving Na/P_i co-transport across the renal brush-border membrane as rate-limiting step, particularly via the Na/P_i co-transporter [1–3]. Mammalian Na/P_i co-transporters have been subdivided into types I–III. The type II Na/P_i co-transporter isoforms (a–c) are the major functional Na/P_i co-transporters [1–3]. The type IIa and IIc co-transporters are expressed in the proximal tubules of the kidney, whereas type IIb is expressed in tissues such as the lung and small intestine [1–3]. Serum phosphate concentrations are maintained within a defined range by expression of type II Na/P_i co-transporters, which is, in turn, regulated by PTH (parathyroid hormone) and vitamin D [1–3]. The actions of vitamin D and PTH are important for the control of intestinal P_i absorption or renal P_i excretion. However, adequate systemic phosphate homoeostasis is likely to require the presence of additional bioactive molecules [1,2].

Studies on patients with tumour-induced osteomalacia and ADHR (autosomal dominant hypophosphataemic rickets) resulted in the identification of FGF23 (fibroblast growth factor 23), a protein that shares sequence identity with other FGFs and which results in hypophosphataemic osteomalacia and inappropriately low serum levels of $1,25(OH)_2D_3$ (1,25-dihydroxyvitamin D_3) [3–6]. The FGF23 protein is a secreted protein of 251 amino acids, including a putative N-terminal signal peptide (residues 1–24) [3,4,6]. ADHR is caused by missense mutations at Arg^{176} and Arg^{179} of FGF23, which are present in the consensus proteolytic cleavage sequence RXXR [3–6]. Since mutations at Arg^{176} and Arg^{179} prevent proteolytic cleavage, a large amount of the mutant protein may escape proteolytic degradation [3,4].

XLH (X-linked hypophosphataemia) is the most common form of inherited rickets, and is caused by inactivating mutations in the *PHEX* (phosphate regulating endopeptidase homologue, X-linked) gene [3,4]. XLH is characterized by hypophosphataemia due to increased renal phosphate clearance, low or inappropriately normal levels of circulating $1,25(OH)_2D_3$ and rickets/osteomalacia [3,4]. Studies have demonstrated high serum levels of FGF23 in patients with XLH; in addition, levels of FGF23 mRNA expression in bone were significantly increased in the Hyp mouse (which is analogous to the human XLH patient), [7,8]. Thus current evidence indicates that FGF23 may be involved in the pathogenesis of XLH.

Continuous exposure to recombinant FGF23 was shown to cause increased renal P_i clearance resulting from decreased renal expression of type II Na/P_i co-transporters [9–14]. These animals showed paradoxically low/normal $1,25(OH)_2D_3$ levels [9–15]. These reports indicate that FGF23 is an important regulator of P_i homoeostasis and vitamin D metabolism.

Vitamin D plays a central role in modulating P_i homoeostasis and P_i uptake by the small intestine and the kidney [1,2]. It is

Abbreviations used: ADHR, autosomal dominant hypophosphataemic rickets; BBMV, brush-border membrane vesicle; FGF, fibroblast growth factor; FGF23M, naked DNA encoding the R179Q mutant of human FGF23; FGF23WT, naked DNA encoding wild-type human FGF23; GAPDH, glyceraldehyde-3-phosphate dehydrogenase; 1α(OH)ase, 25-hydroxyvitamin D_3 1α-hydroxylase; 24(OH)ase, 25-hydroxyvitamin D 24-hydroxylase; $1,25(OH)_2D_3$, 1,25-dihydroxyvitamin D_3; PTH, parathyroid hormone; RT-PCR, reverse transcription–PCR; VDR, vitamin D receptor; XLH, X-linked hypophosphataemia.

[1] To whom correspondence should be addressed: Nutritional Science, Department of Nutrition, School of Medicine, Tokushima University, Kuramoto-Cho 3, Tokushima City 770-8503, Japan (email miyamoto@nutr.med.tokushima-u.ac.jp).

possible that the inappropriately low levels of $1,25(OH)_2D_3$ may suppress the expression of renal and intestinal Na/P_i co-transporters. Indeed, we demonstrated previously that levels of type IIa and type IIb Na/P_i co-transporter proteins were significantly decreased in VDR(−/−) (vitamin D receptor null) mice [16].

Further, targeted ablation of FGF23 [FGF23(−/−) mice] resulted in increased serum phosphate levels and renal phosphate re-absorption, and an elevation in serum $1,25(OH)_2D_3$ levels secondary to enhanced expression of renal 1α(OH)ase (25-hydroxyvitamin D 1α-hydroxylase). These results indicated that FGF23 is essential for normal phosphate and vitamin D metabolism [17]. In contrast, plasma PTH levels were normal, suggesting that hyperphosphataemia in FGF23(−/−) mice occurs via a PTH-independent mechanism [17]. Shimada et al. [14] suggested that FGF23 suppresses renal 1α(OH)ase expression by co-operating or competing with several humoral factors, such as PTH and $1,25(OH)_2D_3$. Thus, while the mechanisms responsible for the high serum phosphate and $1,25(OH)_2D_3$ levels in FGF23(−/−) mice remain unclear, it is possible that high serum $1,25(OH)_2D_3$ levels stimulate the intestinal absorption and renal re-absorption of P_i via the apical Na/P_i co-transporter. This is supported by the fact that levels of the type IIa Na/P_i co-transporter protein were markedly increased in the apical membranes of renal proximal tubule cells in FGF23(−/−) mice [17].

In our previous studies, we examined the effects of administration of FGF23WT (naked DNA encoding wild-type human FGF23) or FGF23M (naked DNA encoding the R179Q mutant of human FGF23) into rats [12]. Injection of FGF23M into rats resulted in significant decreases in plasma P_i levels, renal Na/P_i co-transport activity and type II Na/P_i co-transporter levels. However, injection of FGF23WT into rats had no significant effects. Rats injected with,either FGF23WT or FGF23M highly expressed the human *FGF23* transcript in the liver. The levels of plasma human FGF23 protein were markedly increased in rats injected with FGF23M. However, this was not the case in rats injected with FGF23WT [12]. Thus wild-type FGF23 protein may be degraded in the liver or the blood.

The goal of the present study was to use VDR(−/−) mice to determine (i) whether vitamin D is involved in the regulation of renal P_i re-absorption by FGF23, and (ii) whether the VDR is required for the down-regulation of 1α(OH)ase activity by FGF23.

EXPERIMENTAL

Animals and diet

VDR(−/−) mice were generated by gene targeting as described previously [18]. VDR genotypes were confirmed by analysing the DNA obtained from each mouse approx. 3 weeks after birth. Genomic DNA was extracted from tail clippings and amplified by PCR using primers specific for VDR(+/+) exon 2 or the neomycin-resistance gene, as described previously [16].

VDR(+/+) and VDR(−/−) mice were weaned at 3 weeks of age, and given free access to water and a control diet containing 0.5 % P_i and 0.5 % Ca for 5 weeks. After 5 weeks, naked DNA (encoding FGF23 or FGF23 R179Q) or the empty vector was administered by intravenous injection [12,15].

FGF23 mutant construct and injection of naked DNA

DNA encoding human FGF23 or the FGF23 R179Q mutant was subcloned into the pCAGGS3 expression plasmid vector at a unique EcoRI site between the CAG promoter and a 3′-flanking sequence of rabbit β-globin. The empty pCAGGS3 plasmid (kindly provided by Dr J.-i. Miyazaki, Osaka University, Osaka, Japan) was used as a mock control. Next, 1.5 ml of DNA solution containing 10 μg of each expression plasmid [pCGF23 (wild-type human FGF23), pCGFM2 (human FGF23 R179Q mutant) or pCAGGS3 vector] was administered intravenously, as described previously [12,15]. At 4 days after the injection of naked DNA, blood samples were obtained from the abdominal vein, and tissues were rapidly removed under anaesthesia.

Quantitative analysis of FGF23 mRNA

Total RNA was extracted from the livers of transfected animals using ISOGEN (Nippon Gene, Tokyo, Japan), and cDNA was synthesized using M-MLV (Moloney murine leukaemia virus) Reverse H reverse transcriptase (Superscript; Invitrogen) and an $oligo(dT)_{12-18}$ primer. The amount of human FGF23 cDNA relative to GAPDH (glyceraldehyde-3-phosphate dehydrogenase) cDNA was determined by competitive RT-PCR (reverse transcription–PCR) using a 7700 Sequence Detector (PE Applied Biosystems) [12,15]. The PCR primers used for these experiments did not amplify cDNA of the endogenous mouse FGF23 homologue.

Detection of serum FGF23

The serum concentration of exogenous human FGF23 in mice was determined using the Human FGF23 (C-term) ELISA kit (Immunotopics, San Clemente, CA, U.S.A.), which only detects human FGF23 [12,15]. The serum concentration of endogenous mouse FGF23 was determined using the FGF-23 ELISA kit (KAINOS Laboratories, Inc., Tokyo, Japan). We analysed the cross-reactivity of FGF23 proteins between mouse and human (see Figure 1b). The human FGF-23 (C-term) ELISA kit did not detect endogenous mouse FGF23 in either VDR(+/+) or VDR(−/−) mice. In contrast, the mouse FGF23 ELISA kit clearly detected endogenous mouse FGF23 in both VDR(+/+) and VDR(−/−) mice. Serum FGF23 protein levels were significantly lower in VDR(−/−) than in VDR(+/+) mice. These results indicated that the human FGF23 (C-term) ELISA kit did not cross-react with the endogenous mouse FGF23.

Serum calcium, P_i, PTH and $1,25(OH)_2D_3$ levels

The serum concentrations of Ca^{2+} and P_i were determined by the Calcium-E test and the Phospha-C test (both from Wako, Osaka, Japan) respectively. Serum concentrations of PTH were determined using the mouse PTH ELISA kit (Immunotopics) [16,17]. Serum concentrations of $1α,25(OH)_2D_3$ were determined by a radioreceptor assay (Mitsubishi BCL, Tokyo, Japan) [15].

Northern blot analysis

$Poly(A)^+$ RNA (3 μg/lane) isolated from mouse intestine or kidney was separated on a 1 % (w/v) agarose gel in the presence of 2.2 M formaldehyde and blotted on to a Hybond N^+ membrane (Amersham Pharmacia Biotech) as described previously [12,16,19]. Specific probes for 1α(OH)ase, 24(OH)ase (25-hydroxyvitamin D 24-hydroxylase) and each Na/P_i co-transporter were labelled with [^{32}P]dCTP using the Megaprime DNA Labeling System (Amersham Pharmacia Biotech) [12,16,19]. The specific probes for 1α(OH)ase and 24(OH)ase were similar to those used for RT-PCR. Hybridization proceeded for 3 h at 65 °C, and the blot was evaluated by autoradiography using a Fujix BAS-1500 bioimaging analyser (Fujifilm, Tokyo, Japan).

RT-PCR for 1α(OH)ase and 24(OH)ase

Kidney total RNA extraction and cDNA synthesis were performed as described above. The PCR primers were designed for 1α(OH)ase and 24(OH)ase as follows: 1α(OH)ase (forward/reverse;

5′-3′), CCGCGGGCTATGCTGGAAC/CTCTGGGCAAAGGCAAACATCTGA; 24(OH)ase (forward/reverse; 5′-3′), TGGGAAGATGATGGTGACCC/ACTGTTCCTTTGGGTAGCGT. PCR were performed for 32 cycles, with cycle conditions of 94 °C for 1 min, 58 °C for 1 min, and 72 °C for 1 min. All amplicons were sequenced to confirm the specificity of amplification.

Preparation of BBMVs (brush-border membrane vesicles) and transport assay

BBMVs were prepared from mouse kidney or intestine by the Ca^{2+} precipitation method, as described previously [12,16,19]. BBMV ^{32}P uptake was measured by the rapid filtration technique. A sample of 10 μl of vesicle suspension was added to 90 μl of incubation solution (100 mM NaCl, 100 mM mannitol, 20 mM Hepes/Tris and 0.1 mM $KH_2{}^{32}PO_4$), and the preparation was incubated at 20 °C. Transport was terminated by rapid dilution with ice-cold saline, and the reaction mixture was transferred immediately to a remoistened filter (0.45 μm) and maintained under a vacuum [12,16].

Immunoblotting

Protein samples were heated at 95 °C for 5 min in sample buffer in the presence of 2-mercaptoethanol and subjected to SDS/PAGE. The separated proteins were transferred by electrophoresis to a Hybond-P PVDF transfer membranes and then treated with diluted affinity-purified antibodies against type IIa (1:4000) or type IIc (1:1000) Na/P_i co-transporters [17,18]. Mouse anti-actin monoclonal antibody (CHEMICON) was used as an internal control. Horseradish peroxidase-conjugated anti-rabbit or anti-mouse IgG was utilized as the secondary antibody (Jackson Immuno-Research Laboratories), and signals were detected using the ECL Plus® system (Amersham Pharmacia Biotech) [12,16,19].

Statistical analysis

One-way ANOVA (*post hoc* Scheffé *F*-test) and two-factor factorial ANOVA were performed. Data are expressed as means ± S.E.M. Statistical analysis of endogenous serum FGF23 measurements in VDR(−/−) and VDR(+/+) mice was performed using Welch's test. $P < 0.05$ was considered significant.

RESULTS

Effects of FGF23 on food intake in VDR(+/+) and VDR(−/−) mice

VDR(−/−) and VDR(+/+) mice were weaned at 3 weeks of age, housed in plastic cages, and given free access to water (distilled water) and diet containing 0.5 % calcium and 0.5 % phosphorus for 5 weeks, as described in the Experimental section. We measured the dietary intake of all VDR(−/−) and VDR(+/+) mice used in the study. As shown in Table 1, there were no differences in food intake between VDR(+/+) and VDR(−/−) mice for up to 4 days after the injection of naked DNA.

Expression of mutant FGF23 mRNA and protein

We demonstrated previously that injection of naked DNA plasmids encoding the human *FGF23* gene into animals resulted in the expression of FGF23 protein in the liver for at least 4 days [12,15]. To determine if the effect of FGF23 on intestinal and renal phosphate transport is dependent on vitamin D, naked DNA plasmids encoding the human *FGF23* gene were injected into VDR(+/+) and VDR(−/−) mice. At 4 days after injection, wild-type human FGF23 and mutant FGF23-R179Q mRNAs were present in liver tissue at relatively high levels in both VDR(+/+) and VDR(−/−) mice, as shown by quantitative PCR (Figure 1a).

Using the human FGF23 (C-term) ELISA kit, we demonstrated that protein levels of human FGF23 were markedly increased in both VDR(+/+) and VDR(−/−) mice injected with FGF23M, but not in mice injected with FGF23WT (Figure 1c).

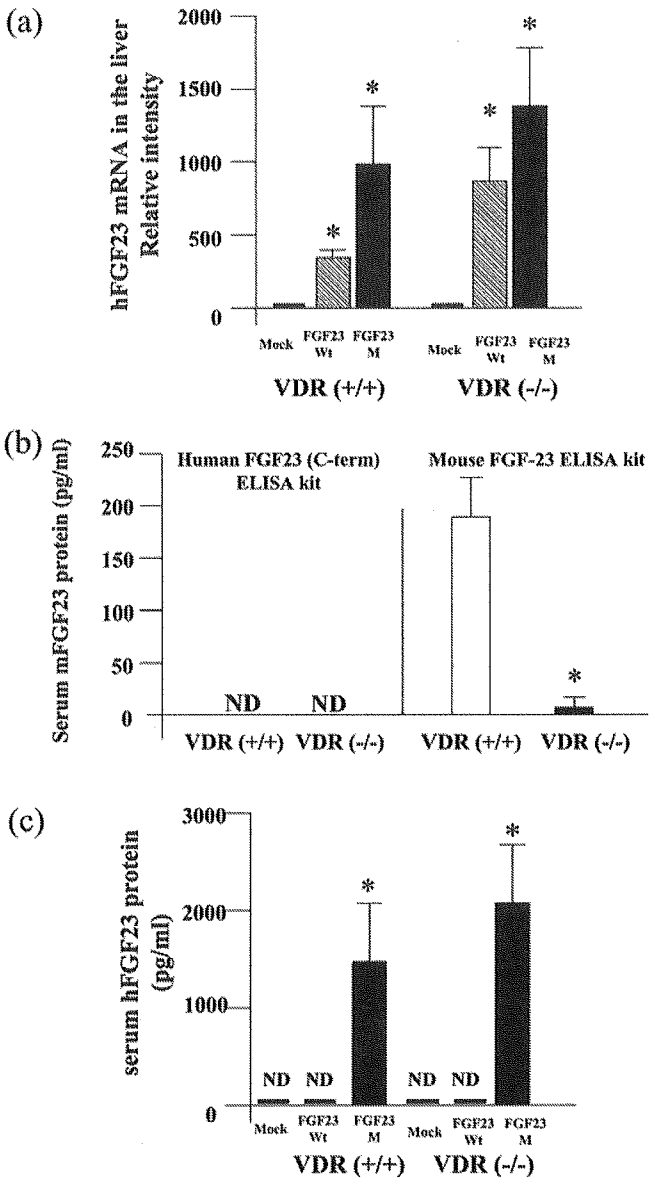

Figure 1 Expression of FGF23 in VDR(+/+) and VDR(−/−) mice

At 4 days after administration of FGF23WT, FGF23M or empty vector to VDR(+/+) mice and VDR(−/−) mice, we analysed the expression of human FGF23 mRNA and protein. (**a**) Expression of FGF23 in the liver, as assessed by competitive RT-PCR (see the Experimental section). FGF23 mRNA levels are shown relative to those of GAPDH mRNA. One-way ANOVA (*post hoc* Scheffé *F*-test) and two-factor factorial ANOVA were performed. Values are means ± S.E.M. ($n = 5$–6); *$P < 0.05$ compared with mock vector control. (**b**) Serum concentrations of endogenous mouse FGF23 (mFGF23) protein in VDR(+/+) and VDR(−/−) mice were determined using two separate ELISA kits, as described in the Experimental section. Statistical analysis of endogenous serum FGF23 levels in VDR(−/−) and VDR(+/+) mice was performed using Welch's test. Values are means ± S.E.M. ($n = 10$); *$P < 0.05$ for VDR(+/+) compared with VDR(−/−) mice. (**c**) Serum concentrations of exogenous human FGF23 protein (hFGF23) were determined by ELISA in VDR(+/+) and VDR(−/−) mice injected with naked DNA. One-way ANOVA (*post hoc* Scheffé *F*-test) and two-factor factorial ANOVA were performed. Values are means ± S.E.M. ($n = 5$–6); *$P < 0.05$ compared with mock vector control. ND, not detected.

Table 1 Effects of FGF23 on food intake in VDR(+/+) and VDR(−/−) mice

One-way ANOVA (*post hoc* Scheffé *F*-test) and two-factor factorial ANOVA were performed. Values are means ± S.E.M. ($n = 6–10$).

			Food intake (g/day)					
Mice	Injection	No. of days of injection ...	−1	0	1	2	3	4
VDR(+/+)	Mock		4.2 ± 0.8	3.6 ± 1.0	4.7 ± 0.9	3.8 ± 0.9	5.3 ± 0.8	4.2 ± 0.8
	FGF23WT		3.9 ± 0.9	3.5 ± 1.1	4.5 ± 0.6	3.7 ± 0.9	5.2 ± 0.8	3.9 ± 0.9
	FGF23M		4.1 ± 0.9	3.8 ± 0.9	4.8 ± 0.5	3.5 ± 0.9	4.7 ± 0.5	4.1 ± 0.9
VDR(−/−)	Mock		4.5 ± 0.8	3.7 ± 1.2	4.3 ± 0.8	3.8 ± 0.8	4.6 ± 0.8	3.9 ± 1.2
	FGF23WT		4.2 ± 0.9	3.9 ± 0.9	4.7 ± 0.6	3.5 ± 1.0	4.9 ± 0.8	3.6 ± 1.0
	FGF23M		4.4 ± 0.8	3.6 ± 0.9	4.2 ± 0.9	4.1 ± 1.1	4.7 ± 0.8	3.5 ± 0.9

Table 2 Effects of FGF23 on serum levels of calcium, P_i, $1,25(OH)_2D_3$ and PTH in VDR(+/+) and VDR(−/−) mice at 4 days after injection

One-way ANOVA (*post hoc* Scheffé *F*-test) and two-factor factorial ANOVA were performed. Values are means ± S.E.M. ($n = 6–10$). Significance of differences: *$P < 0.05$ compared with VDR(+/+) (mock); †$P < 0.005$ compared with VDR(+/+) (FGF23WT); ‡$P < 0.005$ compared with VDR(−/−) (mock); §$P < 0.05$ compared with VDR(−/−) (FGF23WT).

	VDR(+/+)			VDR(−/−)		
	Mock	FGF23WT	FGF23M	Mock	FGF23WT	FGF23M
Calcium (mg/dl)	9.02 ± 0.14	9.03 ± 0.23	9.24 ± 0.24	6.61 ± 0.52*	6.90 ± 0.39	7.46 ± 0.16
P_i (mg/dl)	7.43 ± 0.40	7.43 ± 0.31	5.87 ± 0.16*†	5.73 ± 0.27*	5.12 ± 0.30	3.59 ± 0.36‡§
$1,25(OH)_2D_3$ (pg/ml)	82 ± 16	130 ± 47	6 ± 0.16*†	630 ± 6*	617 ± 16	610 ± 8
PTH (pg/ml)	19.3 ± 3.0	18.5 ± 2.3	16.0 ± 1.0	343 ± 25.9*	281 ± 47.6	277 ± 25.3

Table 3 Effects of injection of FGF23M on intestinal and renal Na^+-dependent P_i transport activity in VDR(+/+) and VDR(−/−) mice

Na^+-dependent P_i co-transport activity was assessed by the measurement of P_i uptake into intestinal or renal BBMVs. One-way ANOVA (*post hoc* Scheffé *F*-test) and two-factor factorial ANOVA were performed. Values are means ± S.E.M. ($n = 5–6$). Significance of differences: *$P < 0.05$ compared with mock; †$P < 0.05$ compared with FGF23WT.

	P_i uptake (nmol/30s per mg of protein)					
	VDR(+/+)			VDR(−/−)		
	Mock	FGF23WT	FGF23M	Mock	FGF23WT	FGF23M
Intestine	0.533 ± 0.03	0.467 ± 0.070	0.304 ± 0.050*†	0.338 ± 0.040	0.364 ± 0.020	0.315 ± 0.060
Kidney	1.024 ± 0.133	0.984 ± 0.100	0.743 ± 0.040*†	1.104 ± 0.171	0.960 ± 0.161	0.733 ± 0.060*†

Effects of FGF23M on serum levels of calcium, P_i, PTH and vitamin D

Serum calcium, P_i, PTH and $1,25(OH)_2D_3$ levels were determined 4 days after injection of FGF23WT, FGF23M or mock vector in VDR(+/+) and VDR(−/−) mice (Table 2). Serum calcium and P_i levels were significantly decreased in VDR(−/−) mice compared with VDR(+/+) mice, as described previously [16,18]. In contrast, serum PTH and $1,25(OH)_2D_3$ levels were markedly increased in VDR(−/−) mice compared with VDR(+/+) mice [16,18]. Injection of FGF23M resulted in a significant decrease in serum P_i, but did not affect serum calcium or PTH, in both VDR(+/+) and VDR(−/−) mice. However, FGF23M resulted in a significant decrease in $1,25(OH)_2D_3$ levels only in VDR(+/+) mice. There were no significant differences in any serum parameter when comparing mice injected with FGF23WT and those injected with mock vector.

Effects of FGF23M on renal and intestinal Na/P_i transport activity in VDR(+/+) and VDR(−/−) mice

We reported previously that intestinal Na/P_i co-transport activity in VDR(−/−) mice was reduced to 60% of that seen in VDR(+/+) mice, and that expression of intestinal Na/P_i co-transporter (type IIb) protein was markedly suppressed in VDR(−/−) mice when compared with VDR(+/+) mice [16]. Further, whereas renal BBMV Na/P_i co-transport activity was similar when comparing VDR(−/−) mice and VDR(+/+) mice, expression of type IIa Na/P_i protein was slightly and significantly decreased in VDR(−/−) mice, and there was no difference in type IIc Na/P_i protein expression between VDR(−/−) and VDR(+/+) mice [16].

In the present study, injection of FGF23M resulted in a significant reduction in intestinal Na/P_i co-transport activity in VDR(+/+) mice, but had no such effect in VDR(−/−) mice (Table 3). Injection of FGF23M also resulted in a significant reduction in renal Na/P_i co-transport activity in both VDR(+/+) and VDR(−/−) mice.

Effects of FGF23M on renal type II Na/P_i co-transporter proteins in VDR(+/+) and VDR(−/−) mice

Injection of FGF23M resulted in significant attenuation of type IIa and type IIc renal Na/P_i co-transporter protein expression in both VDR(+/+) and VDR(−/−) mice (Figures 2I and 2II, left

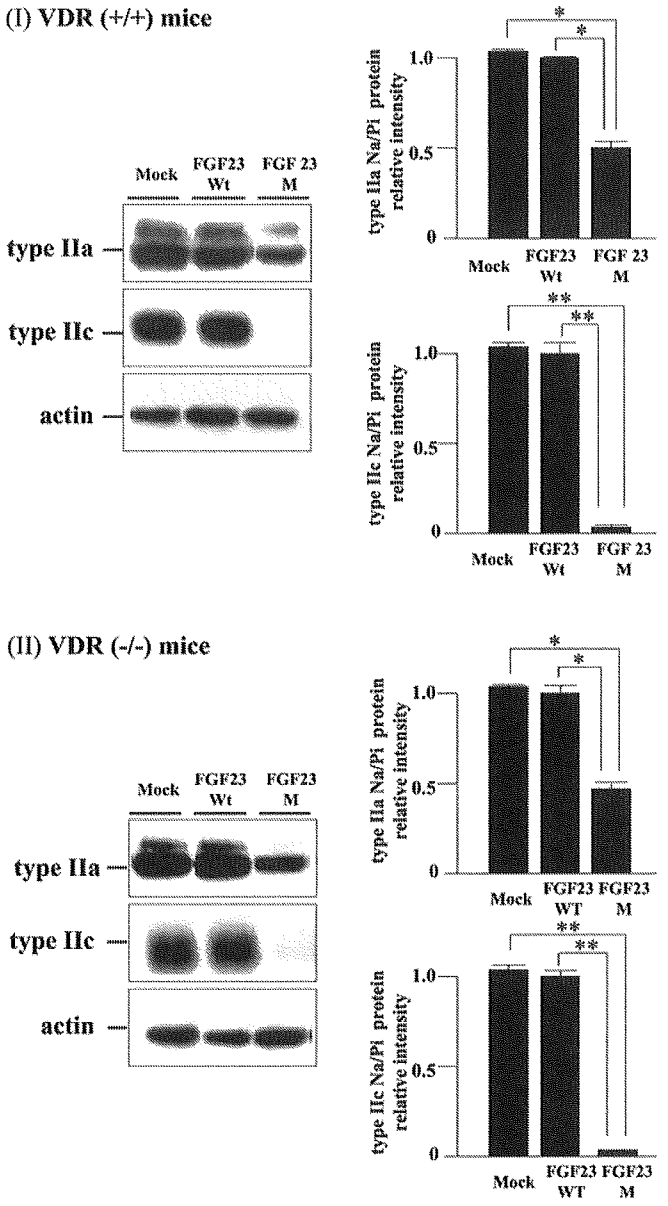

Figure 2 Western blot analysis of renal type II Na/P_i co-transporters

BBMVs (20 μg/lane) isolated from the kidneys of VDR(+/+) and VDR(−/−) mice injected with empty vector, FGF23WT or FGF23M were loaded into each lane. Upper panels, type IIa co-transporter; middle panels, type IIc Na/P_i co-transporter; lower panels, actin (internal control). The immunoreactive band intensity for mice injected with the empty vector was 1.0. One-way ANOVA (*post hoc* Scheffé *F*-test) and two-factor factorial ANOVA were performed. Values are means ± S.E.M. ($n = 5$–6); the significance of differences is indicated by $^*P < 0.05$ and $^{**}P < 0.01$.

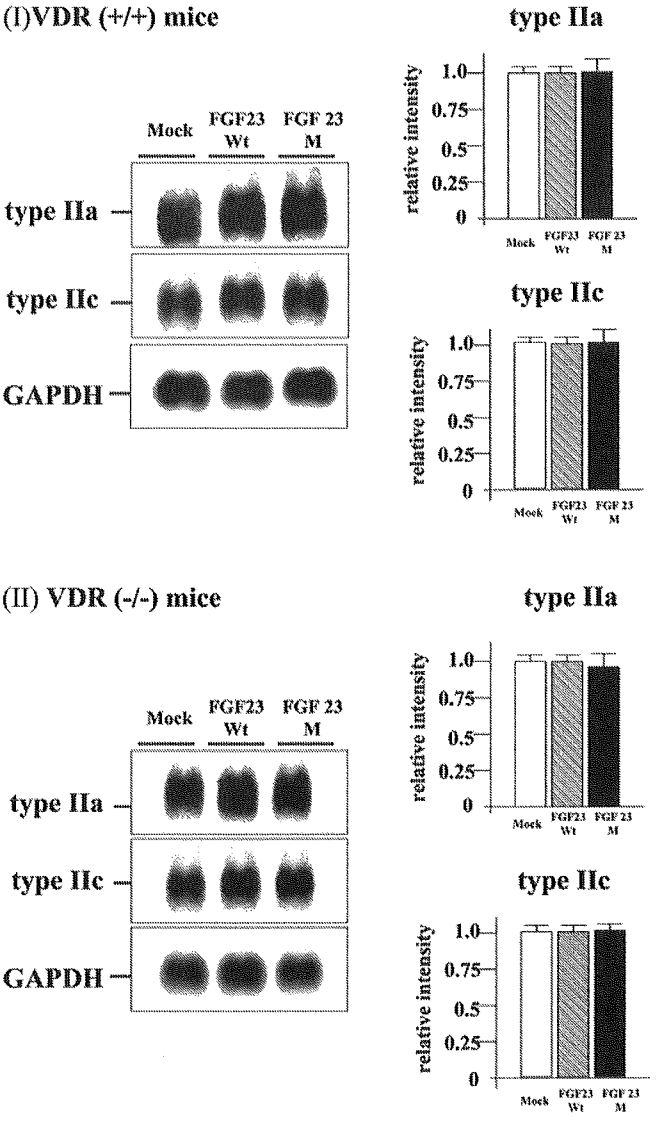

Figure 3 Northern blot analysis of renal Na/P_i co-transporters

Poly(A)$^+$ RNA was extracted from the kidneys of VDR(+/+) and VDR(−/−) mice that had been injected with FGF23WT, FGF23M or the empty vector. Each lane was loaded with 3 μg of RNA. Upper panels, type IIa co-transporter; middle panels, type IIc Na/P_i co-transporter; lower panels, GAPDH (internal control). The visualized band intensity for the mice injected with the empty vector expression was designated as 1.0, and all other band intensities were expressed relative to this value. One-way ANOVA (*post hoc* Scheffé *F*-test) and two-factor factorial ANOVA were performed. Values are means ± S.E.M. ($n = 5$–6).

panels). As shown in Figure 2 (right panels), the levels of type IIa Na/P_i co-transporter protein in BBMVs were decreased to 50% and those of type IIc protein were markedly reduced, compared with BBMVs from mock vector control-injected animals, in both VDR(+/+) and VDR(−/−) mice. However, injection of FGF23M had no effect on type IIa or type IIc transporter mRNA levels in VDR(+/+) or VDR(−/−) mice (Figure 3). As described previously [12,15], injection of mock vector or FGF23WT had no effect on intestinal or renal Na/P_i co-transport activity, or transporter protein or mRNA levels, in VDR(+/+) or VDR(−/−) mice (Table 2, Figures 2 and 3).

Effects of FGF23 on 1α(OH)ase and 24(OH)ase mRNA levels

VDR(−/−) mice have higher 1α(OH)ase mRNA levels and lower 24(OH)ase mRNA levels when compared with VDR(+/+) mice [20,21]. Injection of FGF23M resulted in a marked reduction in 1α(OH)ase mRNA levels (Figure 4) and a significant increase in 24(OH)ase mRNA levels (Figure 4) in both VDR(+/+) and VDR(−/−) mice. However, the increase in 24(OH)ase mRNA levels was much less in VDR(−/−) mice than in VDR(+/+) mice.

DISCUSSION

The present study used VDR(+/+) and VDR(−/−) mice to investigate whether vitamin D is involved in the FGF23-mediated

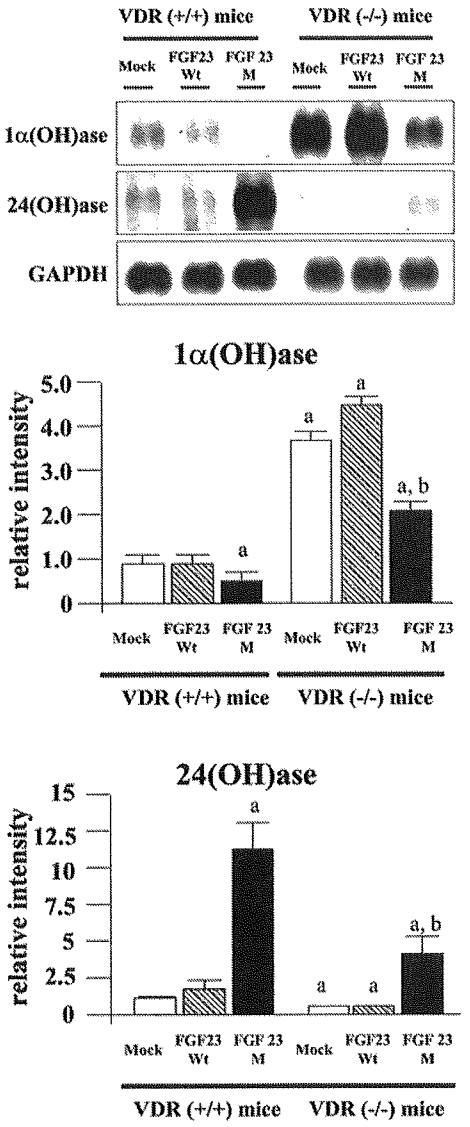

Figure 4 Effects of injection of FGF23M on 1α(OH)ase and 24(OH)ase mRNA levels

Poly(A)$^+$ RNA was extracted from the kidneys of VDR(+/+) and VDR(−/−) mice that had been injected with FGF23WT, FGF23M or the empty vector. Each lane was loaded with 3 μg of RNA. Upper panel, 1α(OH)ase; middle panel, 24(OH)ase; lower panel, GAPDH (internal control). In the histograms, the visualized band intensity for the VDR(+/+) mice injected with the empty vector was designated as 1.0, and all other band intensities are expressed relative to this value. One-way ANOVA (*post hoc* Scheffé *F*-test) and two-factor factorial ANOVA were performed. Values are means ± S.E.M. ($n = 5$–6); $^a p < 0.05$ compared with VDR(+/+) mock vector control., $^b p < 0.05$ compared with VDR(−/−) mock vector control.

regulation of renal P_i re-absorption, and whether the VDR is required for the FGF23-mediated down-regulation of 1,25-$(OH)_2D_3$ levels. The key findings are: (1) VDR may affect the hepatic expression of exogenous FGF23 mRNA, (2) VDR is not involved in the FGF23-mediated suppression of renal Na/P_i co-transport activity, (3) VDR may be involved in the FGF23-mediated down-regulation of intestinal Na/P_i co-transport activity, (4) VDR is involved in the FGF23-mediated induction of renal 24(OH)ase mRNA, and (5) VDR is important in the FGF23-mediated regulation of plasma 1,25$(OH)_2D_3$ levels.

Previous studies demonstrated that injection of FGF23WT into rats resulted in an increase in the hepatic expression of FGF23 mRNA, but not in serum FGF23 levels [12]. This lack of a change in serum FGF23 levels may result from protein degradation of wild-type FGF23 in the liver or the circulation, since rats that received FGF23M showed high levels of mRNA in the liver, and serum FGF23 protein levels also increased. Indeed, the present study demonstrated that wild-type FGF23 was degraded in VDR(+/+) and VDR(−/−) mice. Moreover, the expression of both wild-type and mutant FGF23 in the liver was higher in VDR(−/−) than in VDR(+/+) mice (Figure 1a), which suggests that VDR may control the stability of FGF23 mRNA in the liver. Further studies are needed to clarify the mechanisms underlying the hepatic expression of of FGF23.

Recent studies reported that administration of FGF23 resulted in decreases in type II Na/P_i co-transporter mRNA and proteins levels in the kidney [11,12,14], suggesting that FGF23 may affect the transcriptional step of type II transporter synthesis. However, the present study demonstrated that down-regulation of type II Na/P_i co-transporter expression was not dependent on transcriptionally regulated changes in mRNA. Murer et al. [2] found that changes in type II Na/P_i co-transporter mRNA levels were either rather small or occurred only after prolonged stimulation by thyroid hormone (3,3′,5-tri-iodothyronine) and feeding of a low-P_i diet; furthermore, they occurred after changes in specific transporter protein content, suggesting that changes in mRNA represent a phenomenon secondary to the primary event (i.e. down-regulation or up-regulation of brush border type IIa co-transporter expression) [2]. Thus FGF23 may directly modulate trafficking of the transporter from the apical membrane to the intracellular organelles.

Injection of FGF23M decreased intestinal Na/P_i co-transport activity in VDR(+/+) mice, but not in VDR(−/−) mice, which suggests that the action of the mutant FGF23 on intestinal P_i transport is VDR-dependent. Further, VDR(−/−) mice were characterized by hypophosphataemia, hypocalcaemia and high PTH and 1,25$(OH)_2D_3$ levels, which may also affect the action of FGF23M. In a previous study, we investigated the effects of FGF23 in hypophosphataemic animals (fed a low-P_i diet) [12]. After injection of naked FGF23 DNA, renal Na/P_i co-transport activity and type II phosphate transporter protein levels were significantly deceased in hypophosphataemic rats [12]. 1α(OH)ase mRNA levels and intestinal Na/P_i co-transport activity were also deceased in those animals. These data suggested that hypophosphataemia itself does not affect the function of FGF23 in VDR(−/−) mice. Further investigations aimed at characterizing the regulation of intestinal Na/P_i co-transporter (type IIb) gene expression by VDR and mutant FGF23 would be of benefit.

FGF23 acts to decrease 1α(OH)ase mRNA levels and increase 24(OH)ase mRNA levels. Renal 1α(OH)ase and 24(OH)ase are regulated by several factors, including PTH, calcium, P_i and 1,25$(OH)_2D_3$ [3–5]. In target tissues, 1,25$(OH)_2D_3$ exerts most of its biological actions by binding to the VDR, and feedback regulation of 1α(OH)ase gene expression by 1,25$(OH)_2D_3$ has been reported [22–24]. Thus VDR may be important in the regulation of 1α(OH)ase and 24(OH)ase mRNAs by FGF23.

In the present study, injection of FGF23M induced a decrease in 1α(OH)ase mRNA and an increase 24(OH)ase mRNA levels in both VDR(+/+) and VDR(−/−) mice. These results suggest that the actions of FGF23 are independent of the VDR-mediated decrease in 1α(OH)ase mRNA and increase in 24(OH)ase mRNA. The lack of a decrease in serum 1,25$(OH)_2D_3$ levels in VDR(−/−) mice injected with FGF23M may be for several reasons. First, degradation of 1,25$(OH)_2D_3$ may be insufficient in VDR(−/−) mice, as expression of 24(OH)ase, which is required for the inactivation and degradation of vitamin D metabolites, was relatively low in these mice. Secondly, the serum calcium concentration may directly regulate serum 1,25$(OH)_2D_3$ levels.

Panda et al. [25] studied groups of VDR(−/−) mice exposed to (1) a high-calcium diet, (2) a high-calcium diet plus injection of $1,25(OH)_2D_3$, and (3) a rescue diet (high calcium, high phosphate and high lactose), and showed that only VDR(−/−) mice receiving a rescue diet had normal plasma calcium levels. Further, VDR(−/−) mice had normalized plasma P_i, $1,25(OH)_2D_3$ and PTH concentrations, as well as increased 24(OH)ase mRNA and decreased in 1α(OH)ase mRNA levels [25]. These data suggest that the normalization in serum calcium levels may be related to normalization of serum $1,25(OH)_2D_3$ in mice fed the rescue diet. In the present study, injection of FGF23M did not affect serum calcium levels in either VDR(+/+) or VDR(−/−) mice. Since serum calcium levels remained low in VDR(−/−) mice, high levels of $1,25(OH)_2D_3$ may persist in these mice. Further studies to investigate the FGF23 signalling pathway would be of benefit in clarifying the physiological role of FGF23 in vitamin D metabolism.

In conclusion, the present study has demonstrated that injection of FGF23M lowered renal P_i transport and 1α(OH)ase levels by a mechanism that is independent of the VDR. In contrast, the induction of 24(OH)ase and reduction in serum $1,25(OH)_2D_3$ levels by FGF23 is dependent on the VDR.

We thank Miss Kazuyo Shiozawa for technical support. This work was supported by grants from the Ministry of Education, Science, Sports and Culture of Japan (grants 15790430 to H.S. and 11557202 to K.M.) and the 21st Century COE Program, Human Nutritional Science on Stress Control, Tokushima, Japan.

REFERENCES

1 Miyamoto, K., Segawa, H., Ito, M. and Kuwahata, M. (2004) Physiological regulation of renal sodium-dependent phosphate cotransporters. Jpn. J. Physiol. **54**, 93–102
2 Murer, H., Hernando, N., Forster, I. and Biber, J. (2000) Proximal tubular phosphate reabsorption: molecular mechanisms. Physiol. Rev. **80**, 1373–1409
3 Tenenhouse, H. S. and Sabbagh, Y. (2002) Novel phosphate-regulating genes in the pathogenesis of renal phosphate wasting disorders. Pflugers. Arch. **444**, 317–326
4 Quarles, L. D. (2003) FGF23, PHEX, and MEPE regulation of phosphate homeostasis and skeletal mineralization. Am. J. Physiol. Endocrinol. Metab. **285**, E1–E9
5 The ADHR Consortium (2000) Autosomal dominant hypophosphatemic rickets is associated with mutations in FGF23. Nat. Genet. **26**, 345–348
6 White, K. E., Jonsson, K. B., Carn, G., Hampson, G., Spector, T. D., Mannstadt, M., Lorenz-Depiereux, B., Miyauchi, A., Yang, I. M., Liunggren, O. et al. (2001) The autosomal dominant hypophosphatemic rickets (ADHR) gene is a secreted polypeptide overexpressed by tumors that cause phosphate wasting. J. Clin. Endocrinol. Metab. **86**, 497–500
7 Liu, S., Simpson, L. G., Xiao, Z. S., Burnham, C. E. and Quales, L. D. (2003) Regulation of fibroblastic growth factor 23 expression but not degradation by PHEX. J. Biol. Chem. **278**, 37419–37426
8 Yamazaki, Y., Okazaki, R., Shibata, M., Hasegawa, Y., Satoh, K., Tajima, T., Takeuchi, Y., Fujita, T., Nakahara, K., Yamashita, T. and Fukumoto, S. (2002) Increased circulatory level of biologically active full-length FGF-23 in patients with hypophosphatemic rickets/osteomalacia. J. Clin. Endocrinol. Metab. **87**, 4957–4960
9 Bai, X. Y., Miao, D., Golzman, D. and Karaplis, A. C. (2003) The autosomal dominant hypophosphatemic rickets R176Q mutation in fibroblast growth factor 23 resists proteolytic cleavage and enhances in vivo biological potency. J. Biol. Chem. **278**, 9843–9849
10 Bai, X. Y., Miao, D., Li, J., Golzman, D. and Karaplis, A. C. (2004) Transgenic mice overexpressing human fibroblast growth factor 23 (R176Q) delineate a putative role for parathyroid hormone in renal phosphate wasting disorders. Endocrinology **145**, 5269–5279
11 Larsson, T., Marsell, R., Schipani, E., Ohlsson, C., Ljunggren, O., Tenenhouse, H. S., Juppner, H. and Jonsson, K. B. (2003) Transgenic mice expressing fibroblast growth factor 23 under the control of the α1(I) collagen promoter exhibit growth retardation, osteomalacia and disturbed phosphate homeostasis. Endocrinology **145**, 3087–3094
12 Segawa, H., Kawakami, E., Kaneko, I., Kuwahata, M., Ito, M., Kusano, K., Saito, H., Fukushima, N. and Miyamoto, K. (2003) Effect of hydrolysis-resistant FGF23-R179Q on dietary phosphate regulation of the renal type-II Na/Pi transporter. Pflugers Arch. **446**, 585–592
13 Shimada, T., Mizutani, S., Muto, T., Yoneya, T., Hino, R., Takeda, S., Takeuchi, Y., Fujita, T., Fukumoto, S. and Yamashita, T. (2001) Cloning and characterization of FGF23 as a causative factor of tumor-induced osteomalacia. Proc. Natl. Acad. Sci. U.S.A. **98**, 6500–6505
14 Shimada, T., Hasegawa, H., Yamazaki, Y., Muto, T., Hino, R., Takeuchi, Y., Nakamura, K., Fukumoto, S. and Yamashita, T. (2004) FGF-23 is a potent regulator of vitamin D metabolism and phosphate homeostasis. J. Bone Miner. Res. **19**, 429–435
15 Saito, H., Kusano, K., Kinosaki, M., Ito, H., Hirata, M., Segawa, H., Miyamoto, K. and Fukushima, N. (2003) Human fibroblast growth factor-23 mutants suppress Na^+-dependent phosphate co-transport activity and 1α,25-dihydroxyvitamin D3 production. J. Biol. Chem. **278**, 2206–2211
16 Segawa, H., Kaneko, I., Yamanaka, S., Ito, M., Kuwahata, M., Inoue, Y., Kato, S. and Miyamoto, K. (2004) Intestinal Na/Pi cotransporter adaptation to dietary Pi content in vitamin D-receptor (VDR) null mice. Am. J. Physiol. Renal Physiol. **287**, F39–F47
17 Shimada, T., Kakitani, M., Yamazaki, Y., Hasegawa, H., Takeuchi, Y., Fujita, T., Fukumoto, S., Tomizuka, K. and Yamashita, T. (2004) Targeted ablation of FGF23 demonstrates an essential physiological role of FGF23 in phosphate and vitamin D metabolism. J. Clin. Invest. **113**, 561–568
18 Yoshizawa, T., Hanada, Y., Uematsu, Y., Takeda, S., Sekine, K., Yoshihara, Y., Kawakami, T., Akioka, K., Sato, H., Ushiyama, Y. et al. (1997) Mice lacking the vitamin D receptor exhibit impaired bone formation, uterine hypoplasia and growth retardation after weaning. Nat. Genet. **6**, 391–396
19 Ohkido, I., Segawa, H., Yanagida, R., Nakamura, M. and Miyamoto, K. (2003) Cloning, gene structure and dietary regulation of the type-IIc Na/Pi cotransporter in the mouse kidney. Pflugers Arch. **446**, 106–115
20 Li, X., Zheng, W. and Li, Y. C. (2003) Altered gene expression profile in the kidney of vitamin D receptor knockout mice. J. Cell. Biochem. **89**, 709–719
21 Takeyama, K., Kitanaka, S., Sato, T., Kobori, M., Yanagisawa, J. and Kato, S. (1997) 25-Hydroxyvitamin D3 1a-hydroxylase and vitamin D synthesis. Science **277**, 1827–1830
22 Barletta, F., Dhawan, P. and Christakos, S. (2004) Integration of hormone signaling in the regulation of human 25(OH)D3 24-hydroxylase transcription. Am. J. Physiol. Endocrinol. Metab. **286**, E598–E608
23 Christakos, S., Dhawan, P., Liu, Y., Peng, X. and Porta, A. (2003) New insights into the mechanisms of vitamin D action. J. Cell. Biochem. **88**, 695–705
24 Christakos, S., Barletta, F., Huening, M., Dhawan, P., Liu, Y., Porta, A. and Peng, X. (2003) Vitamin D target proteins: function and regulation. J. Cell. Biochem. **88**, 238–244
25 Panda, D. K., Miao, D., Bolivar, I., Li, J., Huo, R., Hendy, G. N. and Goltzman, D. (2004) Inactivation of the 25-hydroxyvitamin D 1alpha-hydroxylase and vitamin D receptor demonstrates independent and interdependent effects of calcium and vitamin D on skeletal and mineral homeostasis. J. Biol. Chem. **279**, 16754–16766

Received 26 October 2004/25 April 2005; accepted 10 May 2005
Published as BJ Immediate Publication 10 May 2005, doi:10.1042/BJ20041799

JB Minireview—Reproductive / Urogenital Organ Development and Molecular Genetic Cascades *J. Biochem.* **138**, 105–110 (2005)
DOI: 10.1093/jb/mvi118

Study of Androgen Receptor Functions by Genetic Models

Takahiro Matsumoto[1,2], Ken-ichi Takeyama[1], Takashi Sato[1] and Shigeaki Kato[1,2,*]

[1]Institute of Molecular and Cellular Biosciences, University of Tokyo, 1-1-1 Yayoi, Bunkyo-ku, Tokyo, 113-0032; and [2]ERATO, Japan Science and Technology Agency, 4-1-8 Honcho, Kawaguchi, Saitama, 332-0012

Received April 6, 2005; accepted April 20, 2005

Androgens exert most of their biological activities through binding to the androgen receptor (AR). The AR belongs to the nuclear receptor superfamily and acts as a ligand-inducible transcriptional factor. AR dysfunction causes a diverse range of clinical conditions, such as testicular mutation (Tfm) syndrome, prostate cancer, and spinal and bulbar muscular atrophy (SBMA). However, the molecular basis of the AR function underlying these AR-related disorders remains largely unknown due to the lack of stable genetic models. Here we review recent results of our studies into genetic models of the loss of AR function in mice and the gain of AR function in *Drosophila*.

Key words: androgen receptor (AR), androgen receptor knockout (ARKO), *Drosophila*-eye model, polyQ repeat, spinal and bulbar muscular atrophy (SBMA), testicular feminization mutation (Tfm).

Abbreviations: AR, androgen receptor; ARE, androgen response element; KO, knockout; SBMA, spinal and bulbar muscular atrophy; Tfm, testicular feminization mutation.

Androgens as male sex hormones have a critical role in wide rage biological processes (*1*, *2*). These include spermatogenesis, virilization of genitalia and brain functions. Most actions of androgens are mediated by the nuclear androgen receptor (AR), which acts as ligand-inducible transcription factor (*3*, *4*). Liganded AR forms homodimers and binds specific DNA elements in the target gene promoter. The DNA element that binds AR is the common sequence 5′-AGAACANNNTGTTCT-3′, referred to as the consensus androgen response element (*ARE*). To date, a number of clinical disorders of the AR have been reported. Classical AR functional abnormalities cause a spectrum of disorders of androgen insensitivity syndrome (AIS) or testicular feminization mutation (Tfm) (*5–9*). AR mutations underlying these disorders include amino acid substitutions in the DNA or ligand binding domains, point mutations leading to premature stop codons, and deletions of the AR gene (*6*, *8*, *9*). In addition, expansion of a polyQ repeat region within AR has been implicated in the pathogenesis of a motor neuron disease called spinal and bulbar muscular atrophy (SBMA) (*5*, *7*). AR is a relatively large protein compared to other steroid receptors, due to its long N-terminal A/B domain that contains this polyQ repeat. However, the molecular basis of AR function underlying these AR-related disorders remains largely unknown due to the lack of stable genetic models. In this article, we present recent results of our studies into genetic models of loss of AR function in mice (*10–12*) and gain of AR function in *Drosophila* (*13*).

*To whom correspondence should be addressed at: Institute of Molecular and Cellular Biosciences, University of Tokyo, Yayoi, Bunkyo-ku, Tokyo 113-0032. Fax: +81-3-5841-8477, Tel: +81-3-5841-8478, E-mail: uskato@mail.ecc.u-tokyo.ac.jp

Domain features of androgen receptor

In the late 1980s, the cloning the human AR opened an avenue for understanding the molecular mechanism of androgen actions (*14*). The AR gene comprises eight exons that encode a 110-kDa protein. In common with other members of the nuclear receptor superfamily, the AR contains distinct structural and functional domains referred to as domains A to E(F) (*3*, *4*). The highly conserved middle region (C domain) acts as a DNA binding domain, while the ligand binding domain (LBD) is located in the C-terminal E/F domain. The LBDs of most nuclear receptors, including AR, have been analyzed and are comprised of 12 α helixes that form a pocket to capture cognate ligands (*15*, *16*). Upon ligand binding, the C-terminal α helix 12 (H12) in the LBD shifts position to create a space, with helixes 3 to 5 serving as the key interface following dissociation of corepressor complexes and association of coactivator complexes (*3*, *17*). During ligand-induced transactivation, the N-terminal domains A/B and the steroid receptor LBD act as interacting regions for the co-activator complexes. The autonomous activation function-1 (AF-1) within the A/B domain is ligand-independent, while AF-2 within the LBD is induced upon ligand binding (*18*). While unliganded LBD appears to suppress the function of the A/B domain, ligand binding to the LBD is thought to evoke LDB function and restore A/B domain function through an as yet undescribed intramolecular alteration of the entire steroid receptor structure.

Generation of AR-null mutant mice by gene targeting using the Cre-loxP system

Although androgens seem to exert beneficial effects in males, the physiological role of AR-mediated androgen signaling in male physiology and behaviors has not been established. This is because estrogens are locally converted from serum androgens by aromatase in target

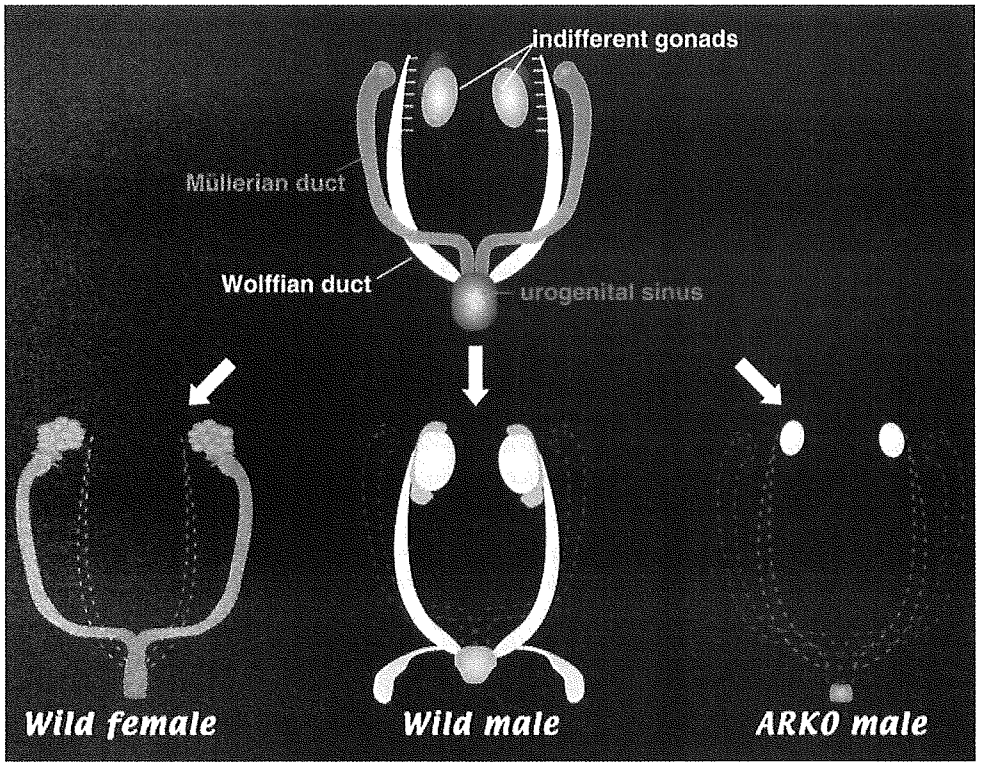

Fig. 1. **Schematic representation of reproductive organs in male ARKO mice.** Male ARKO mice are characterized by female-typical appearance, including a clitoris-like phallus and a vagina with a blind end, as well as the absence of internal male and female reproductive organs, except for the presence of atrophic testes.

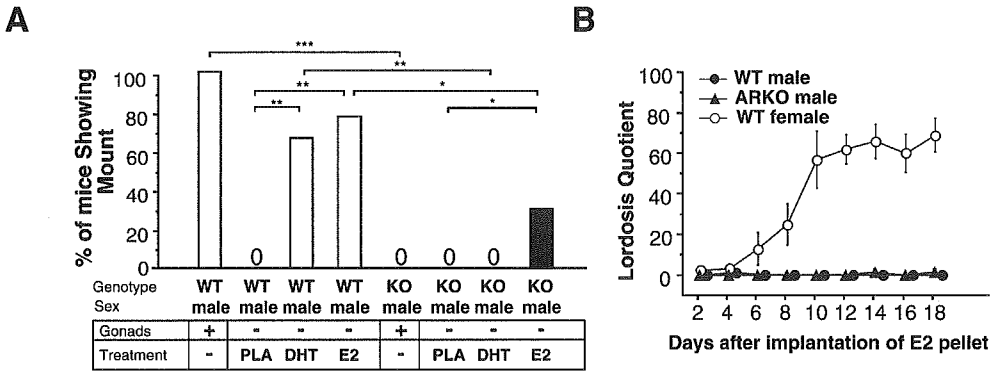

Fig. 2. **Ablation of AR in male mice resulted in the lack of both male and female sexual behaviors.** (A) Loss of all components of male sexual behavior in intact (Gonads: +) 10-week-old ARKO mice. (B) Lordosis was not induced in gonadectomized ARKO male mice after treatment with E2. (C) Schematic representation of AR function in perinatal brain masculinization and defeminization.

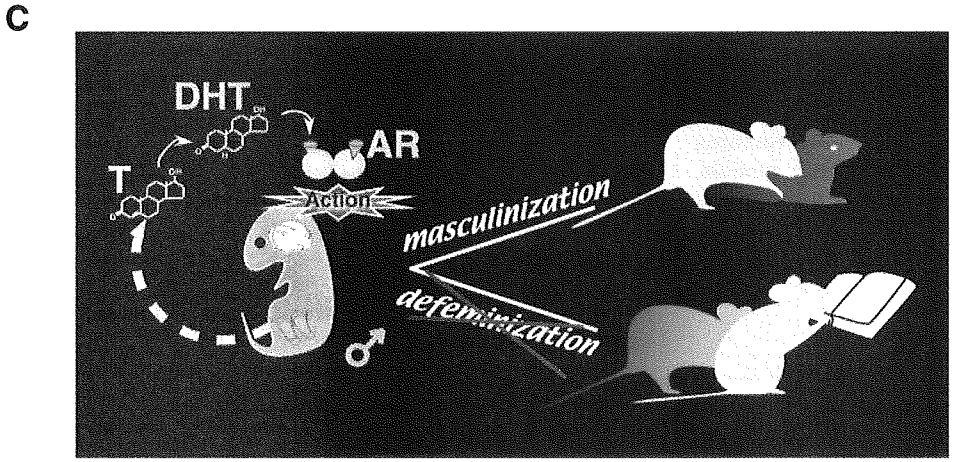

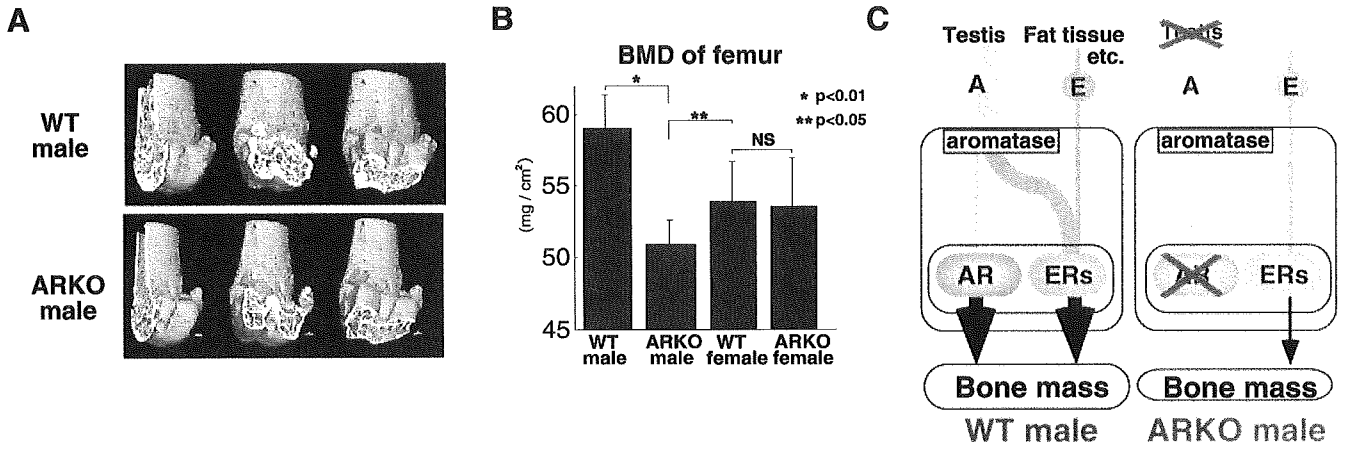

Fig. 3. **Osteopenia in male ARKO mice.** (A) Three-dimensional computed tomography images of distal femora from representative 8-week-old male ARKO mice. (B) Bone loss in femur of 8-week-old male ARKO mice by BMD analysis. (C) Schema of skeletal sex hormone action.

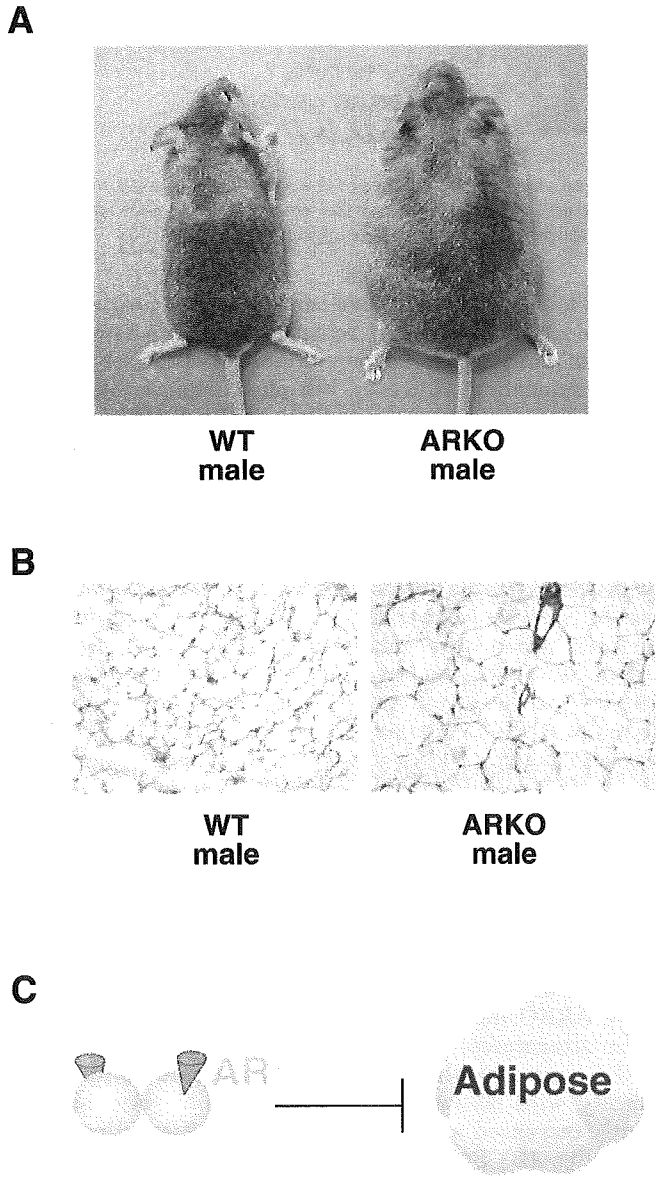

organs. The AR gene is located on the X chromosome, and therefore exists as a single copy in males. As male animals lacking a functional AR gene would be expected to show Tfm abnormalities with complete infertility, successful targeted disruption of the AR gene, essential for reproduction, necessarily prohibits its transmission to the next generation. Therefore, to define AR function, an AR-null mutant mouse line was generated by means of the Cre-loxP system (*19*), which was used to circumvent the problem of male infertility. We first generated floxed AR mice, in which the AR gene locus was flanked by loxP sites. Floxed AR mice were fully fertile and showed normal expression of AR protein. We then crossed these mice with mice that expressed the Cre recombinase ubiquitously under the control of a CMV promoter, and obtained male and female ARKO mice at theoretical Mendellian frequencies. No AR transcript or protein was detected, which indicates that they were complete null mutant mice for the AR gene.

Tfm abnormalities in male ARKO mice

As expected, the AR-null mutation in males resulted in the ablation of masculinization of reproductive organs (*11*). ARKO mice exhibited female-typical external appearance, including a vagina with a blind end and a clitoris-like phallus, instead of a penis and scrotum (Fig. 1). Male reproductive organs, such as seminal vesicles, vas deferens, epididymis and prostate were absent in ARKO males. However, no ovaries or uteri were observed, although small inguinal testes were present. Histological examination of the testes showed that spermatogenesis was severely arrested. These observations in ARKO males are similar to a human hereditary disorder, AIS or Tfm, in which mutations in the AR gene have been identified in several families. Testicular androgen levels were very low, whereas serum estrogen levels appeared normal in ARKO males.

Fig. 4. **Late onset of obesity in male ARKO mice.** (A) External appearance of 30-week-old male ARKO mice. (B) Subcutaneous white adipose tissues from 30-week-old male ARKO mice. (C) Schema of AR function in adipogenesis.

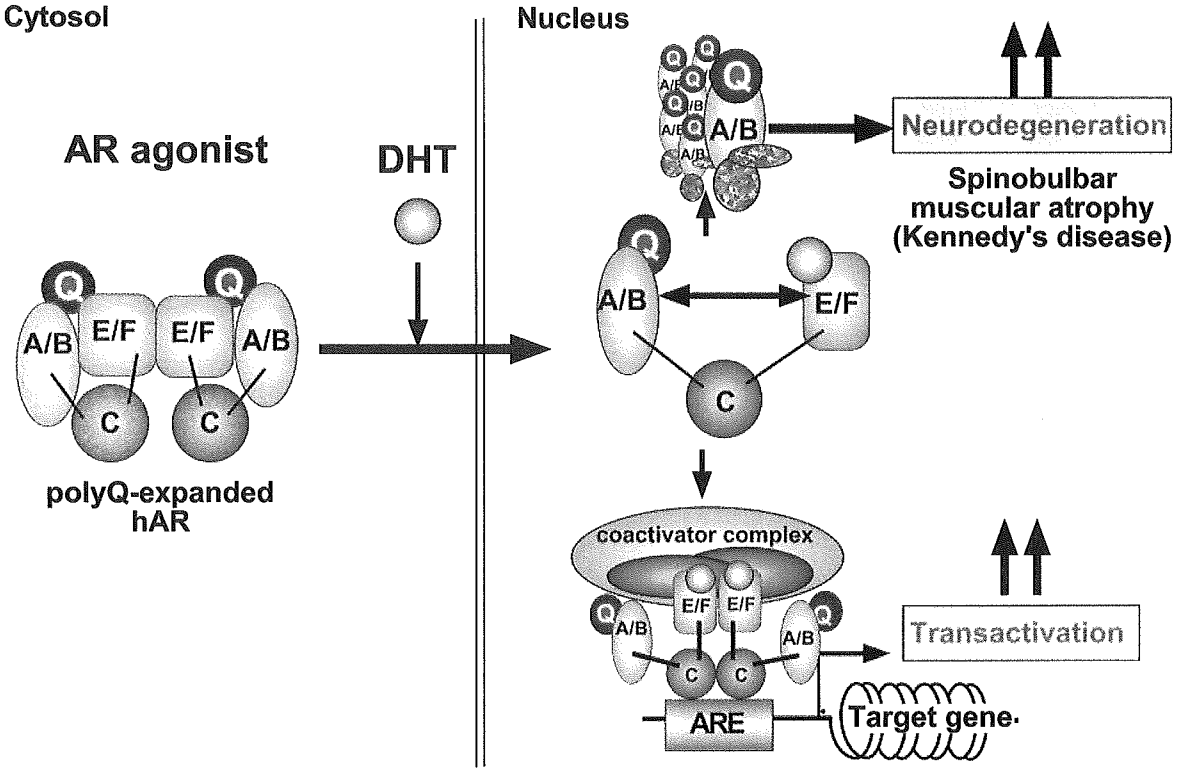

Fig. 5. **Androgen-dependent structural alteration by the polyQ-expanded human AR.** It is considered that the polyQ-expanded AR is inactive in the transactivation without the agonists (androgens); but in the presence of the agonists, it alters the molecular structure and also recruits the co-activators, while the polyQ repeat induces apoptosis by their aggregation.

Brain masculinization requires AR function

Next, we investigated the AR function in perinatal brain masculinization (*11*). Intact ARKO males showed no male sexual behaviors and impaired male aggressive behaviors (Fig. 2A). Treatment with the non-aromatizable androgen 5α-dihydrotestosterone (DHT) partially rescued impaired male aggressive behaviors in ARKO males, suggesting that DHT activity in male aggressive behaviors is mediated via both AR-independent and -dependent pathways in the adult. In contrast, no female sexual behavior was induced in ARKO males even when estrogen alone or both estrogen and progesterone was administered (Fig. 2B), suggesting that the brains of ARKO males were defeminized (Fig. 2C). The AR function in brain masculinization at a limited perinatal stage was further studied in ARKO females. While DHT-induced masculinization of female brain at the perinatal stage led to adult female mice sensitive to both E2 and DHT with the expression of male-typical behaviors, such responses were completely abolished in ARKO females. These data provide genetic evidence that once the brain is perinatally masculinized through liganded-AR, the sexually developed brain becomes sensitive to both androgen and estrogen with regard to the expression of male-typical behaviors in adulthood (Fig. 2C).

High turnover osteopenia in male ARKO mice

Beyond the reproductive physiology, sex steroid hormones are implicated in involvement of homeostatic processes, such as bone metabolism. Sex hormone status is reflected in bone mass, and hormonal deficiency is well known to lead to progressive bone loss. The most striking example, osteoporosis in postmenopausal women, is a state of estrogen deficiency coupled with imbalanced bone remodeling. However, the physiological role of the AR-mediated androgen signaling in the skeletal tissues has not yet been established. We performed in vivo analyses of the bone of 8-week-old ARKO males and found that the trabecular and cortical bone volumes were remarkably reduced (Fig. 3, A–B) (*12*). Bone loss in ARKO mice was only partially prevented by treatment with aromatizable testosterone (Fig. 3C). Histomorphometric analysis further showed that both bone formation and resorption were enhanced in ARKO males, but the increase in bone resorption exceeded that in formation. In view of these findings, we concluded that bone loss found in ARKO males was based on the high bone turnover osteopenia.

Late onset of obesity in male ARKO mice

Another hallmark of ARKO males was late-onset obesity (Fig. 4A) (*10*). From birth, ARKO male mice were externally indistinguishable from normal female WT littermates in terms of ano-genital distance and growth curve up to 10 weeks. However, thereafter, the growth of ARKO males rapidly increased, and at 12 weeks of age, male ARKO mouse body weights exceeded that of WT male littermates. This late onset of drastically increased ARKO male growth curve led to the clear development of obesity, with 30-week old ARKO males showing significantly increased wet tissue weights in white adipose tissues (Fig. 4B). Such clear increases were not detected in